Evaluating the Reliability of Grain-size Sorting for Organic Biomarker Analysis

J. S. Hingley [1], P. S. Bray [1], T. Agterhuis [1], G. L. Foster [1], B. S. Wade [2], J. H. Whiteside [1,3,] and G. N. Inglis [1]

[1]School of Ocean and Earth Science, National Oceanography Centre Southampton, University of Southampton, UK

[2]Department of Earth Sciences, University College London, UK

[3]Department of Earth and Environmental Sciences, San Diego State University, USA

Corresponding authors: Joe Hingley (j.hingley@soton.ac.uk), Gordon Inglis (gordon.inglis@soton.ac.uk)

Key Points:

- We investigate the potential of using grain-size sorted marine sediments for biomarker analysis.
- GDGT distributions are consistent regardless of grain-size sorting, and fine-grained sediment fractions are most suitable for temperature reconstruction.
- Leaf wax distributions differ among various grain-size fractions which can bias proxy reconstructions.

Abstract

Organic and inorganic geochemical proxies are fundamental for interpreting past climate variability. For inorganic analysis, marine sediments are often size fractionated to isolate foraminifera, while organic analysis employs subsamples of bulk sediment. Although previously sieved sediments could be used for biomarker analysis, this approach and potential methodological biases have not been assessed in pre-Holocene sediments. Here we explore lipid biomarkers (isoGDGTs, brGDGTs, *n*-alkanes) across grain-size fractions in Cenozoic-aged marine sediments, assessing whether sieved sediments can be used to reconstruct paleoenvironmental change. We analyse biomarkers in fine (<63 μm) and coarse (>63 μm) grain-size fractions and compare various proxy metrics with those in bulk sediments. Our findings reveal a strong linear correlation between TEX_{86} in different size-fractions and bulk sediment (r^2 = 0.85-0.94, both p <0.001), indicating sea surface temperature reconstructions are viable using previously sieved sediments. MBT'_{5ME} shows a weaker yet significant correlation between fine and bulk sediment (r^2 = 0.70-0.81, both p <0.001). In fine fractions, *n*-alkanes typically reflect the bulk sediment composition, whereas coarse sediments consistently underestimate bulk sediment chain length metrics, suggesting organo-mineral associations. Our results demonstrate GDGT-based temperature proxies can typically be analysed using sieved sediments, whilst *n*-alkanes can be influenced by organo-mineral associations and contamination during processing. We assessed contamination from traditional processing techniques, determining sieving sediments into plastic beakers can introduce hydrocarbon contamination but this does not affect GDGT analysis. Our study confirms that archives of fine-grained sediment fractions can be resurrected for GDGT analysis, encouraging a re-examination of global stores of processed samples.

Plain Language Summary

Geochemical proxies in marine sediments are used to understand how Earth's climate has changed over time. Typically, sediment samples are separated by grain size for inorganic analyses, while organic analyses use the whole, unsorted sample. However, many sediment samples have already been sieved for past studies and are considered unviable for organic analyses. In this study, we analysed biomarkers in fine (<63 μm) and coarse (>63 μm) sediment fractions from Cenozoic-aged (up to 66 million years old) marine sediments. We focused on key

biomarkers used to reconstruct sea surface temperature (SST), terrestrial temperature (MAT) and the vegetation community. We found that SST and MAT estimates from both size fractions typically match those from bulk sediment, suggesting sieved sediments can still provide reliable temperature records. However, plant waxes in different grain size fractions often differed from bulk sediments and are less reliable. This is likely related to how these lipids adhere to minerals. Our results show that many previously processed sediment samples can still be used to extract meaningful climate data. However, we found that using plastic containers during sieving can introduce contamination and thus outline best practices to utilise grain-size sorted sediments for future biomarker analysis.

1. Introduction

Organic and inorganic geochemical proxies obtained from marine sediments provide insights into Earth's climatic and environmental history across various timescales (e.g., Auderset et al., 2022; Judd et al., 2024). Inorganic geochemical analysis usually involves separating sediments into size fractions - typically coarse (> 63 µm) and fine (< 63 µm) - to isolate foraminifera and finer carbonates necessary for subsequent trace element and isotopic analysis, including $\delta^{18}O$ (Metcalfe et al., 2019), Mg/Ca (Barker et al., 2005) and $\delta^{11}B$ (Crumpton-Banks et al., 2022). In contrast, organic biomarker analysis is typically conducted using a separate bulk sediment subsample. However, this approach increases the demand for increasingly limited sediment material. This can be partially resolved by analysing lipid biomarkers prior to conducting grain-size separation and subsequent inorganic geochemical analysis. A previous study by Crumpton-Banks et al. (2022) evaluated Miocene-age marine sediments from three oceanographic regions (the western equatorial Atlantic, the North Atlantic and the west Tasmania Margin) and demonstrated that alkenone distributions and $\delta^{11}B$ values from planktonic foraminifera can be analysed sequentially using the same sediments. However, thousands of 'legacy' sediments have already been sieved into different size fractions for inorganic analysis and are thus typically considered unsuitable for lipid biomarker analysis.

Organic carbon (OC) tends to be closely associated with fine-grained (<63 µm) minerals that have high surface areas (i.e., clays and silt) (Hemingway et al., 2019). However, it remains unclear whether organic-based sea surface temperature (SST) proxies (e.g., TEX_{86}, U^{K}_{37}') differ

systematically between fine- and coarse-grained marine sediment fractions. In the South Yellow Sea, alkenone and isoprenoid GDGT distributions have been shown to vary between grain-size sorted sediment fractions and bulk sediment (Xiao et al., 2023). When these variations are converted to SST, there is an average discrepancy of ~±3 °C for TEX_{86} and ±5 °C for U^{K}_{37}' (Xiao et al., 2023). Similarly, in various continental margin sediments, long-chain alkyl diol distributions deviate between grain-sized sorted sediment fractions and bulk sediments. When translated into SST using the long-chain diol index (LDI), fine fraction sediments yield SSTs more representative of the bulk sediment (average ±1.8 °C in the fine silt fraction) compared to the more variable coarse fraction (average ±3.5 °C in the coarse silt fraction) (Lattaud et al., 2022), suggesting that fine-grained sediment fractions yield more robust organic geochemical measurements.

The impact of grain-size sorting on different terrestrial biomarker proxies remains uncertain. Although branched GDGTs do not show a selective association with either grain-size fraction in marine sediments from the Gulf of Mexico (Yedema et al., 2024), the influence of grain-size fractionation on the MBT'_{5ME} mean annual air temperature proxy is not yet known. Long-chain *n*-alkanes, used to assess organic matter source and thermal maturation, exhibit strong absorption to clay minerals due to their relatively hydrophobic nature (Kusch et al., 2021). However, the distribution of *n*-alkanes in marine sediments is highly variable, influenced by physical mechanisms, indicating no universal pattern to *n*-alkane grain-size distributions (Liu et al., 2013).

It is thus crucial to better understand how various terrestrial and marine biomarkers are distributed amongst different sediment size fractions and whether grain-size sorted sediments are suitable for paleoclimate reconstruction. Here we studied marine sediments (n = 39 from a diverse range of Cenozoic (66 million years to present) marine depositional environments (Fig. 1). We test the hypothesis that lipid biomarker distributions in ancient marine sediments are preferentially associated with fine-grain sediments (< 63 μm). To achieve this, we developed a methodological framework to determine the distribution of various terrestrial and marine biomarkers in fine (<63 μm) and coarse (>63 μm) sediment grain fractions and then compared our results to bulk unsieved sediments to quantify the deviations between sediment grain-sizes.

Additionally, we evaluated potential contamination from conventional processing methods and identify best practices for using legacy marine sediments in biomarker analysis moving forward.

2 Materials and Methods

2.1 Study sites

Integrated Ocean Drilling Program (IODP) Site U1356 is situated offshore of Wilkes Land (63.3102°S, 135.9989°E) and spans the early Pleistocene to late Paleocene. Five samples were obtained from the mid Eocene (approx. 46 – 48 Ma). This site represents a high latitude environment with a water depth of 3992 m (Escutia et al., 2011). The lithology is dominated by bioturbated and calcareous claystone with a moderately high organic carbon content (~1.0 to 1.4%).

IODP Site U1451 is situated on the Bengal Fan (8.011°N, 88.747°E). Six samples were obtained from the Early Miocene to late Eocene (~ 20 to 35 Ma). The lithology is dominated by micaceous siliciclastic sediment with large turbidite deposits throughout the Oligocene and a moderate-to-low organic carbon content (<1%) with water depth of 3600 m representing a deep ocean ridge environment (France-Lanord et al., 2016).

Ocean Drilling Program (ODP) Site 1218 is located in the equatorial Pacific (8.988°N, 135.366°W) and spans the Pleistocene to middle Eocene. Five samples were obtained from across the Oligocene (23-34 Ma) representing an open ocean equatorial environment with modern water depth of 4200 m (Shipboard Scientific Party 2002). The lithology is dominated by nannofossil ooze and has low organic carbon content (< 0.1%).

ODP Site 1168 is situated on the south coast of Australia (42.610°S, 144.413°E) and spans the Late Pliocene to late Eocene. At Site 1168, 10 samples were spanning the Quaternary to the earliest Oligocene (0.1-34 Ma). This site represents a high southern latitude shallow coastal environment. The lithology into the Oligocene is dominated by sandstone with a moderate-to-

low organic carbon content (<1%), with a water depth of 800 m at the start of the Oligocene (Shipboard Scientific Party, 2001a).

ODP Site 1172 is also situated on the south coast of Australia (43.960°S, 149.928°E) and spans the Pleistocene to the Cretaceous. Eight samples were obtained encompassing the late Eocene to Palaeocene (~34 to ~60 Ma). This site represents a high southern latitude deep coastal environment. The lithology is dominated by calcareous biogenic pelagic oozes with a moderately high organic carbon content (1.0 to 1.5%). This site is situated at a water depth of 2620 m (Shipboard Scientific Party, 2001b).

Deep Sea Drilling Project (DSDP) Site 242 is located in the Mozambique Channel (15.851°S, 41.823°E) and spans the Quaternary to late Eocene, with a modern water depth of 2275 m (Shipboard Scientific Party, 1974). This site represents a coastal deep water environment. Five samples were obtained from across the Oligocene section. The lithology is dominated by clayey nannofossil chalk (Shipboard Scientific Party, 1974).

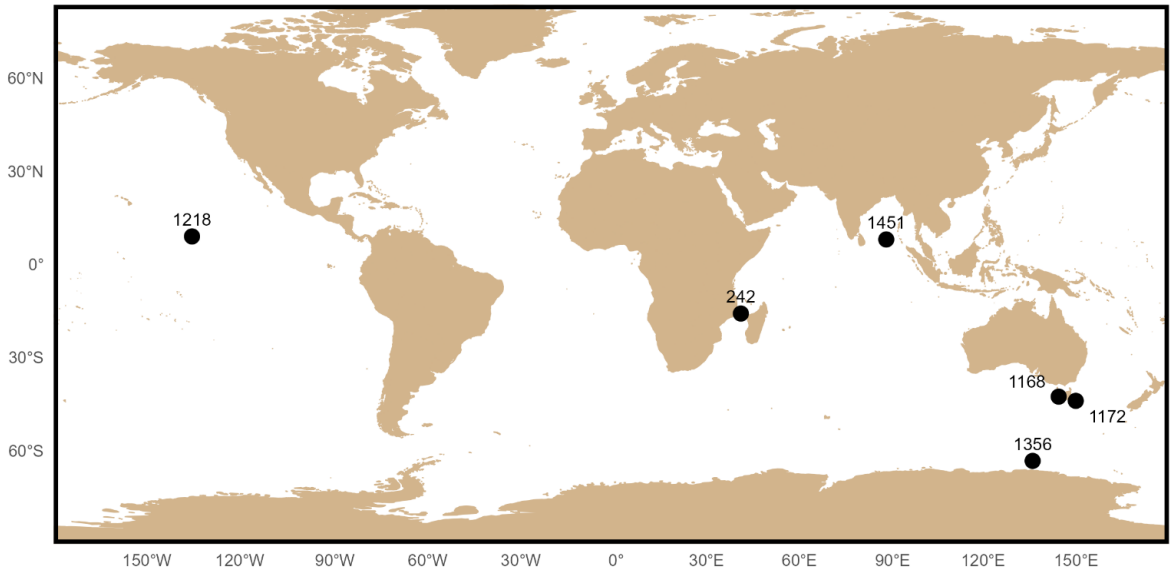

Fig. 1: Map of modern location of sites studied. Made with *R Natural Earth.*

2.2 Experimental Framework

A total of 39 sediment samples were processed at the Organic Geochemistry Laboratories at the University of Southampton. Samples were freeze-dried for 48 hours and then partially crushed with a rubber mallet, following the methods outlined by Crumpton-Banks et al. (2022). Samples were kept in the original sample bag to prevent any contamination from the mallet. To ensure consistency with previous studies (Peterse and Eglinton, 2017; Xiao et al., 2023), approximately half of each sediment sample was separated into fine (<63 µm) and coarse (>63 µm) fractions (Fig. 2) using 2 L of milliQ water. Individual sieves were rinsed with dichloromethane (DCM):Methanol (MeOH) (9:1 *v*/*v*) both before and after the sieving process. The fine fraction (<63 µm) was left to settle for ~1 week in a furnaced glass beaker, after which excess water was siphoned off. Samples were then oven dried for seven days at 40 °C to remove any remaining water and homogenised using a pestle and mortar to increase surface area for extraction (Fig. 2). Oven-drying was chosen instead of freeze-drying to ensure consistency with previous studies (e.g., Arrigoni et al., 2024, Boltovskoy and Wright, 1976, Synder and Huber, 1996). The coarse fraction (>63 µm) was dried under the same conditions, then carefully removed from the sieve with a spatula and homogenised. The control sediment, which was composed of the remaining ~50% of each sample, was oven dried under the same conditions to ensure consistency.

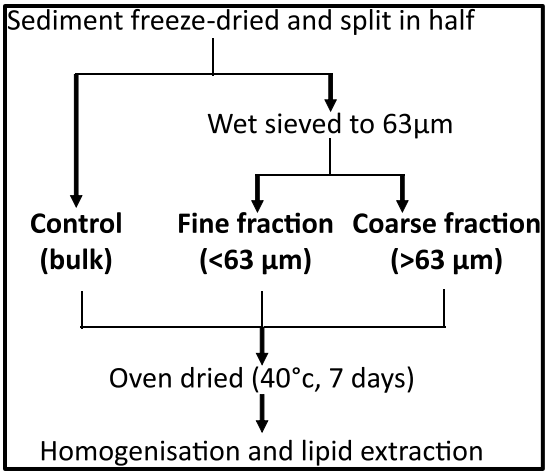

Fig. 2: Protocol for evaluating the impact of grain-size sorting upon lipid biomarker distributions in Cenozoic-aged marine sediments.

2.3 Additional cleaning and disaggregation experiments

During grain-size sieving, the fine fraction (< 63 µm) is often collected in a plastic beaker. However, plastic breakers are comprised of hydrocarbons and other chemical additives (Andrady and Neal, 2009) and commonly introduce contaminants into processed biomarker samples, and are avoided during organic processing. To evaluate this further, furnaced sand was sieved into glass and plastic (polypropylene) beakers and extracted following methodologies outlined in Section 2.4. We also carried out an identical experiment using a single sediment sample from ODP Site 1168 (Supplementary Fig. 1) to evaluate the impact of plastic contamination on marine sediment.

Inorganic geochemical studies sometimes use sodium hexametaphosphate (commonly known as Calgon) as a disaggregating agent, but the consequent impact on biomarker analysis has not been studied. To explore this further, a method blank comprised of sand and kaolin (2:1 w/w) was prepared (spiked with two internal standards: bromo-hexadecane and hyocholic acid) and dispersed in a 9:1 (*v*/*v*) dilution of MilliQ water and Calgon, and shaken for 14 days to replicate sediment disaggregation. The material was then sieved and dried prior to extraction following the methodologies outlined in Section 2.3.

2.4 Organic Geochemistry

2.4.1 Extraction and separation

Bulk, fine (<63 μm) and coarse (>63 μm) sediments (1g – 30g depending on sample availability and mass fraction) were extracted using Accelerated Solvent Extraction (Thermo ASE 350) at the University of Southampton using 9:1 (*v*/*v*) DCM:MeOH at 100 °C over 3 x 15 min extraction cycles at 1,500 PSI. The total lipid extract (TLE) was then dried under a gentle stream of nitrogen (N_2). Separation into apolar (containing *n*-alkanes), ketone and polar fractions (containing isoGDGTs and brGDGTs) was achieved using silica column chromatography by elution with 4 mL Hexane:DCM (9:1, *v*/*v*), 4 ml Hexane:DCM (1:1, *v*/*v*) and 4 ml DCM:MeOH (1:1, *v*/*v*) respectively. Fractionated lipid extracts were then stored at -20 °C until analysis. A procedural blank comprising a blend of sand and kaolin was sieved and extracted after every 10 samples following identical protocols.

2.4.2 GC-MS analysis

Long-chain *n*-alkanes were analysed using a ThermoFisher Trace 1310 gas chromatograph (GC) coupled to a Thermo TSQ8000 Triple Quadrupole mass spectrometer (MS/MS). An Agilent DB-5 column (30 m × 0.25 mm internal diameter, 0.25 μm film thickness) was used to achieve separation with helium as the carrier gas. The GC oven programme began at 40 °C for 2 minutes, before increasing to 310 °C at 6 °C min^{-1} and held at 310 °C for 15 minutes. Measurement was achieved using full scan (50-650 Da) and selective ion monitoring (SIM mode) using m/z = 57 (characteristic *n*-alkane fragment ion). An in-house standard measured after every ten samples was used to monitor long-term instrument stability.

2.4.3 LC-MS analysis

Polar fractions (containing isoGDGTs and brGDGTs) were filtered through a 0.45 μm PTFE filter and analysed using Ultra-High-Performance-Liquid-Chromatography-Mass-Spectrometry (UHPLC-MS) using an Agilent 1260 UHPLC coupled to a 6130 single quadrupole MSD using SIM in normal phase separation. Normal phase separation was achieved using two UHPLC columns (BEH HILIC columns, 2.1 x 150 mm, 1.7 μm) following Hopmans et al. (2016) using *n*-hexane (solvent A) and *n*-hexane:isopropanol (IPA) 9:1 (*v*/*v*) (solvent B). Separation was

achieved using 18% solvent B for 25 min, increasing to 35% solvent B over 25 mins, then 100% solvent B over 30 mins, for one minute before returning to 18% solvent B over 19 mins to equilibrate the column prior to the next injection. SIM was used to scan for the following ions: *m*/*z* 1022, 1020, 1018, 1036, 1034, 1032, 1050, 1048, 1046, 1302, 1300, 1298, 1296, 1294, and 1292. Rounded GDGT masses were monitored, and thus a small bias in absolute BIT values may be introduced (Davtian et al., 2018). An in-house standard reference material containing abundant isoGDGTs was analysed after every 10 samples. The instrumental uncertainty of the marine standard was ±0.01 TEX_{86} units. Relative abundance of GDGTs was obtained using Agilent ChemLabs software.

2.5 GDGT-based biomarker proxies

The relationship between isoGDGT cyclisation and SST is quantified using TEX_{86} (Schouten et al., 2002):

$$TEX_{86} = \frac{[GDGT-2] + [GDGT-3] + [Cren']}{[GDGT-1] + [GDGT-2] + [GDGT-3] + [Cren']} \quad \text{Eq.1}$$

TEX_{86} values are converted into SST using a linear Bayesian regression model (BAYSPAR) (Tierney and Tingley, 2014). BAYSPAR uses a modern core-top dataset to find modern analogues with similar TEX_{86} values and determines a regression value based on these analogues. Where possible, priors were based upon existing temperature records from the same site or inferred from published nearby SST records (Supplementary Table 2).

The MBT'_{5Me} is used to quantify mean air temperature (MAT) (De Jonge et al., 2013; Weijers et al., 2007).

$$MBT'_{5ME} = \frac{[\mathrm{Ia} + \mathrm{Ib} + \mathrm{Ic}]}{[\mathrm{Ia} + \mathrm{Ib} + \mathrm{Ic} + \mathrm{IIa} + \mathrm{IIb} + \mathrm{IIc} + \mathrm{IIIa}]} \quad \text{Eq.2}$$

MBT'_{5ME} values are converted to terrestrial surface temperatures using the BAYMBT Bayesian regression model (Dearing Crampton-Flood et al., 2020), Where possible, priors were based

upon existing temperature records from the same site or inferred from published nearby mean annual temperature (MAT) records (Supplementary Table 2).

The cyclisation of branched tetraethers (CBT) index (Weijers et al., 2007) quantifies the pH dependence of the distribution of 6-methyl brGDGTs (Eq.3).

$$CBT = -\log\left(\frac{[\mathrm{Ib} + \mathrm{IIb}]}{[\mathrm{Ia} + \mathrm{IIa}]}\right) \quad \text{Eq.3}$$

The branched-isoprenoid tetraether (BIT) index is used to determine the relative input of brGDGTs (predominantly soil-derived) versus isoGDGTs (predominantly marine-derived) (Hopmans et al., 2004).

$$BIT = \frac{[\mathrm{Ia} + \mathrm{IIa} + \mathrm{IIa}' + \mathrm{IIIa} + \mathrm{IIIa}']}{[\mathrm{Ia} + \mathrm{IIa} + \mathrm{IIa}' + \mathrm{IIIa} + \mathrm{IIIa}' + \mathrm{Crenarchaeol}]} \quad \text{Eq.4}$$

BIT index values can range from 0 to 1, with values closer to zero indicating minimal brGDGT input, and thus representative of marine organic matter. Values closer to 1 indicate elevated terrestrial input, with BIT values >0.4 typically considered to bias TEX_{86} values (Weijers et al., 2006). Although brGDGTs are predominantly produced by soil (acido)bacteria, in-situ marine production can also occur in shallow marine sediments (Xiao et al., 2016).

2.6 Leaf wax-based biomarker proxies

Terrestrial plants synthesise long-chain *n*-alkanes with an odd-over-even predominance (Eglinton and Hamilton, 1967). With increasing thermal maturity, odd-numbered *n*-alkanes gradually degrade, leading to a lower odd-over-even predominance. The thermal maturity of long-chain *n*-alkanes was quantified using the carbon preference index (CPI) (Bray and Evans, 1961).

$$CPI = \frac{1}{2}\left[\left(\frac{\sum_{odd}(C_{25-31)}}{\sum_{even}(C_{26-32)}}\right) + \left(\frac{\sum_{odd}(C_{27-33)}}{\sum_{odd}(C_{26-32)}}\right)\right] \quad \text{Eq.5}$$

Thermally immature sediments exhibit higher CPI values (typically >3-30, Bush and McInerey, 2013) whereas thermally mature, degraded *n*-alkane distributions exhibit lower CPI values closer to 1.

The average chain length (ACL) evaluates the dominance of different long-chain *n*-alkane chain lengths (Poynter and Eglinton, 1990) and is the weighted average of higher chain *n*-alkanes. This has been used to distinguish between different plant communities (e.g., moss vs non-mosses, Bush and McInerney, 2013) and is defined as follows (Eq. 6):

$$ACL = \frac{25(nC_{25}) + 27(nC_{27}) + 29(nC_{29}) + 31(nC_{31}) + 33(nC_{33})}{nC_{25} + nC_{27} + nC_{29} + nC_{31} + nC_{33}} \quad \text{Eq. 6}$$

3 Results

3.1 Bulk sediment biomarker distributions

3.1.1 Isoprenoid GDGT distributions

IsoGDGTs were detected in 30 out of 39 bulk sediment samples, specifically those from Site U1451 (n = 4 out of 5 samples), Site 242 (n = 5 out of 5 samples), Site U1356 (n = 3 out of 5 samples), Site 1168 (n = 10 out of 10 samples) and Site 1172 (n = 8 out of 8 samples). At Site 1218 (n = 5), isoGDGT abundance was below the limit of detection. The isoGDGT distribution at Site 1168 is dominated by crenarchaeol (38-52% relative abundance) and isoGDGT-0 (27-42%). At Site 1172, the isoGDGT distribution is dominated by isoGDGT-0 (20-37%) and crenarchaeol (45-54%). At Site U1356, the isoGDGT distribution is dominated by crenarchaeol (51-59%) and isoGDGT-0 (16-28%). The isoGDGT distribution at Site U1451 is dominated by crenarchaeol (47-65% relative abundance). At Site 242, isoGDGT-0 is abundant (27-53%), with a variable abundance of crenarchaeol (9% to 46%).

3.1.2 Branched GDGT distributions

brGDGTs were detected in 26 out of 39 bulk sediment samples, specifically those from in Site U1451 (3 out of 4), Site 242 (5 out of 5 samples), Site 1168 (10 out of 10 samples) and Site 1172 (8 out of 8 samples). At Site U1356 and Site 1218 the brGDGT abundance was below the limit of detection in all samples. At Site U1451, the brGDGT distribution is dominated by tetramethylated brGDGTs (81-86% of the brGDGT distribution). At Site 1168, the brGDGT distribution varies downcore. In the younger samples (2 – 15 Ma) the distribution is dominated by tetra- and pentamethylated brGDGTs (21-35% and 28-38% to total brGDGT distribution respectively), whilst older samples are dominated by tetramethylated brGDGTs (60-79% of total brGDGT distribution). At Site 1172 the brGDGT distribution is almost entirely comprised of tetramethylated brGDGTs (61-89% relative abundance). At Site 242, the brGDGT distribution is entirely comprised of 5-methyl brGDGTs, with no 6-methyl brGDGTs above the limit of detection.

3.1.3 SST and MAT estimates in bulk sediments

In Site 1168, bulk sediment TEX_{86}-derived SSTs show a gradual cooling from 28 °C in the earliest Oligocene (~32 Ma) to 18 °C during the Quaternary (~2.5 Ma), with a short-lived increase to 30 °C during the Middle Miocene Climatic Optimum (~15 Ma). At Site 1172, bulk sediment TEX_{86}-derived SSTs increase during the latest Paleocene-to-earliest Eocene and peak during the early Eocene Climatic Optimum (30 °C) with a gradual decline thereafter. Bulk sediment TEX_{86} SST at Site U1451 estimates remain similar across all samples (28.4 °C ± 0.9 °C). At Site 242 bulk sediment TEX_{86} SST estimates are variable (22°C – 36°C) and BIT indices are high (BIT = >0.96 in all 5 samples).

In Site 1168, MBT'_{5ME}-derived MAT estimates show ~10 °C of cooling from the late Oligocene (25 °C) to Quaternary (15 °C) (Supplementary Fig. 3). At Site 1172, there is a gradual increase in MAAT during the latest Paleocene-to-early Eocene with maximum MAATs during the EECO to 29 °C, before gradually cooling to 24 °C in the late Eocene (Supplementary Fig. 3). At Site

U1451, MBT'_{5ME} -derived MAT estimates average ~27-28 °C. At Site 242, MAT is very variable across all 5 samples ranging from 10.9 °C to 19.5 °C with no obvious long term trend.

3.1.4 Long-chain *n*-alkane distributions and chain length metrics

Long-chain *n*-alkanes were detected in 25 out of 39 bulk sediment samples. Site 1218 has very poor *n*-alkane preservation (n = 2 out of 5 samples). Where *n*-alkanes were detected, the abundance is dominated by higher chain *n*-alkanes with an average CPI of 2.8. Site 1172 (n = 8 out of 8 samples) contains mid and long chain *n*-alkanes (average ACL = 29.2) and is dominated by the long chain *n*-alkanes, with an odd-over-even predominance consistent with input from higher plants (average CPI = 2.0). Site U1451 (n = 4 out of 4 samples) contains predominantly long chain *n*-alkanes, with lower abundances of mid and short chain *n*-alkanes, consistent with input from higher plants (average CPI = 3.2, ACL = 30.1). Site U1356 (3 out of 4 samples) is dominated by long chain *n*-alkanes (average ACL = 28.8), with a high CPI (average CPI = 3.1), consistent with input of thermally immature organic matter.

3.2 Lipid biomarker distributions in different grain-size fractions

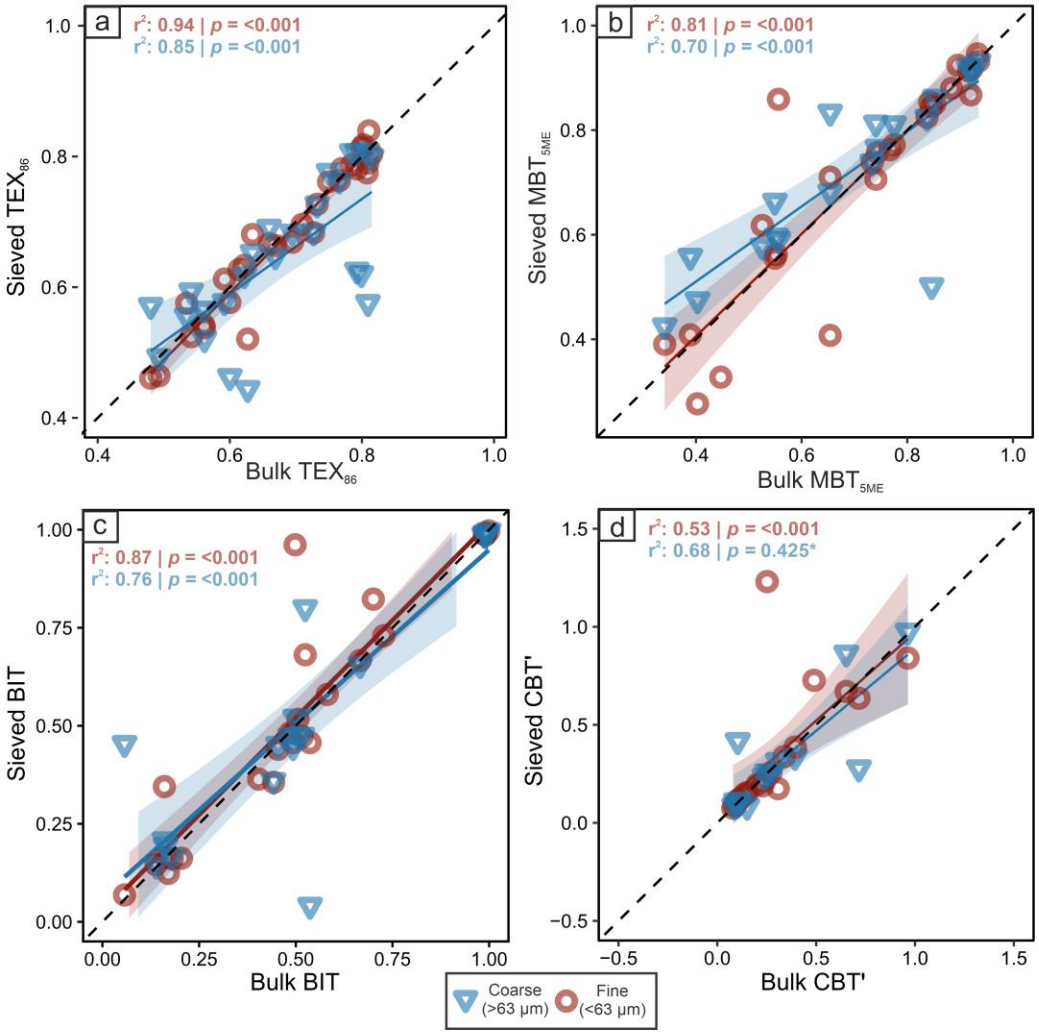

Fig. 3: Comparison of bulk sediment isoGDGT and brGDGT indices and the fine (<63 µm, red circles) and coarse (>63 µm, blue triangles) fractions for **a)** TEX_{86}, **b)** MBT'_{5ME}, **c)** BIT and **d)** CBT. Dashed line indicates 1:1 ratio. Coloured bands represent 95% confidence intervals (blue = coarse fraction i.e. >63 µm and red = fine fraction, i.e. <63 µm). * indicates not statistically significant.

3.2.1 TEX_{86}-derived SST estimates

TEX_{86} values from both the fine and coarse size fractions show little deviation from the bulk sediment (fine = ±0.05 TEX_{86} units, coarse = ±0.14 TEX_{86} units), with a statistically significant linear correlation between both grain-size fractions and bulk sediment (fine: $r^2 = 0.94$, p = <0.001, coarse: $r^2 = 0.85$, p = <0.001, Fig. 3.a.). Deviation from the bulk sediment is larger than

347 the instrumental uncertainty of 0.01 TEX_{86} units, but when translated into SST, the fine and
348 coarse size fractions are within the calibration uncertainty except for 1 fine fraction outlier and 5
349 coarse outliers (Supplementary Fig. 2).

350

351 3.2.2 MBT'_{5ME} -derived MAT estimates

352 MBT'_{5ME} values from both the fine and coarse size fractions vary across different sites. At Site
353 1172 and Site U1451, MBT'_{5ME} values in the fine and coarse size fractions are similar to the bulk
354 sediment (<±0.05 MBT units, Fig. 3.b.) and across all sites there is a strong linear relationship
355 between grain-size sorted sediment and the bulk sediment (fine $r^2 = 0.81$, $p = <0.001$, coarse $r^2 =$
356 0.70, $p = <0.001$). However, at Site 1168, MBT'_{5ME} values deviate by up to 0.34 MBT units and
357 when converted into MAT, this deviation is large (up to ±7.1 °C).

358

359 3.2.3 BIT Index

360 In Site 1172, BIT indices across all grain-sizes show relatively minimal deviation from bulk
361 sediment (<0.12 BIT units), whereas at both Site 1168 and Site U1451, the BIT exhibits
362 relatively high deviation from bulk sediment (up to 0.3 and 0.5 BIT units respectively,
363 Supplementary Fig. 6). Overall, the variation of BIT values is consistent across grain-size, but in
364 some samples there are relatively, and significant, large fluctuations (Fig 3.c.).

365

366 3.2.4 CBT Index

367 brGDGT-derived CBT values are variable across sites and show a linear correlation (fine: $r^2 =$
368 0.53, $p = <0.001$, coarse: $r^2 = 0.68$, $p = 0.425$ (not significant), Fig. 3.d.). At ODP Site 1168,
369 CBT indices are highly variable (up to ±1.3 CBT units) whereas CBT values in Site 1172 are
370 more representative of bulk sediment (± 0.04 CBT units). When converted into pH values, Site
371 1172 has a deviation of ±0.03 pH and Site 1168 deviates by ± 2.00 pH.

372

3.2.5 *n*-alkane Chain Length Metrics

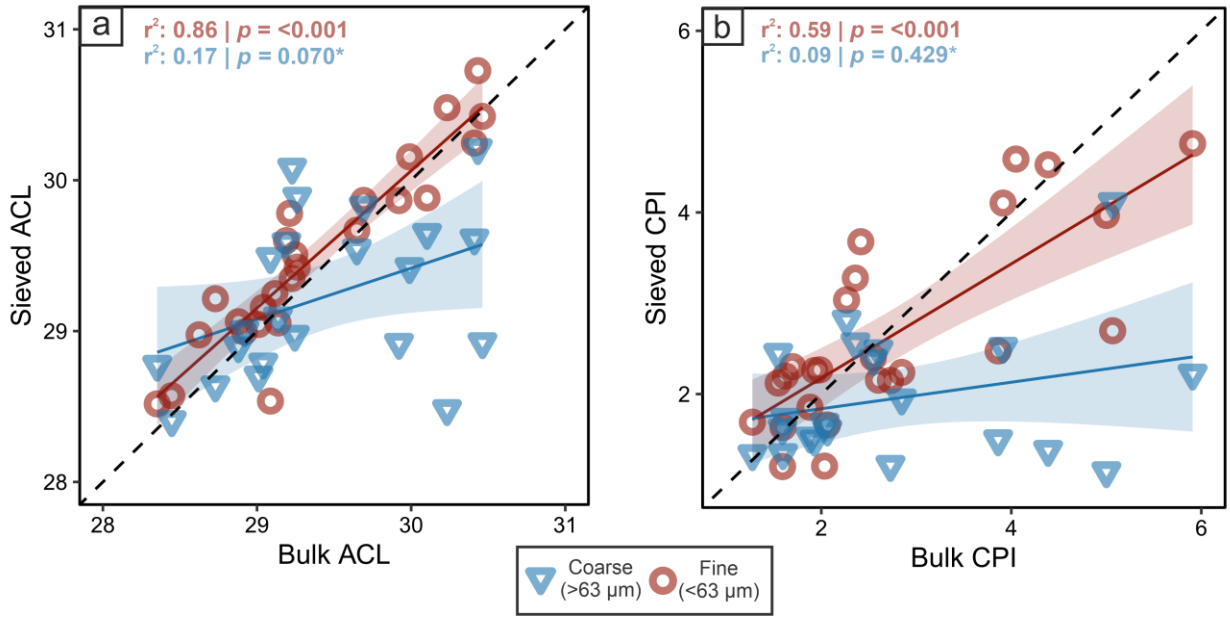

Fig. 4. Comparison of *n*-alkane chain length metrics in bulk sediment compared to fine (<63 µm, red circles) and coarse (>63 µm, blue triangles) fractions for **a)** Average Chain Length and **b)** Carbon Preference Index. Dashed line indicates 1:1 ratio. Coloured bands represent 95% confidence intervals. * indicates not statistically significant.

The average chain length (ACL) of the fine fraction across all sites shows less deviation from the bulk sediment (r^2 = 0.86, = <0.001, with a mean difference of ± 0.2 ACL units) than the coarse fraction (±0.5 ACL units, r^2 = 0.17, p = 0.070, Fig 4.a.). However, at Site 1168, ACL values in the fine fraction can deviate from the bulk sediment up to 1.8 ACL units (Supplementary Fig. 4). Across all sites, CPI values in bulk sediment range from 1.3 to 5.9. CPI values in fine-grained sediment fractions deviate from bulk sediments by up to 2.4 CPI units (Supplementary Fig. 5) but overall there is a linear correlation between CPI in bulk sediment and fine grain sizes (r^2 = 0.59, p = <0.001). In coarse-grained sediment fractions, the CPI deviates by up to 3.9 CPI units from bulk sediment. This is not a significant relationship (r^2 = 0.09, p = 0.429) but in most samples the CPI in coarse grain sizes systematically underestimates bulk sediment values (Fig. 4.b.).

3.3 Contamination experiments

To independently evaluate the contribution of contamination from sieving procedures, blends of furnaced sand and clay were sieved both conventionally and using an idealised sieving protocol

393 (solvent cleaning sieves and furnaced glass labware). Sieving furnaced sand (Fig. 5) or marine
394 sediments (Fig. 6) into glass beakers introduced no detectable contamination (
395 Fig. 5.a, red line). In contrast, when furnaced sand (Fig. 5) was sieved into a plastic beaker,
396 extensive contamination was introduced into fine grained sediment fractions (<63 µm)(
397 Fig. 5.a, black line). Specifically, an unresolved complex mixture (UCM) is detected within the
398 *n*-alkane-containing apolar fraction and represents a series of isotactic alkanes likely to originate
399 from plastic beakers. The GDGT-containing polar fraction was unaffected by plastic
400 contamination as this analysis uses selected ion monitoring (SIM) (Supplementary Fig. 1).
401 Calgon is often used to disaggregate sediment and may also introduce contamination. We find
402 low-level contamination in Calgon treated samples associated with an unresolved complex
403 mixture (UCM) in the fine fraction (
404 Fig. 5.b) and no obvious contamination in the coarse fraction.

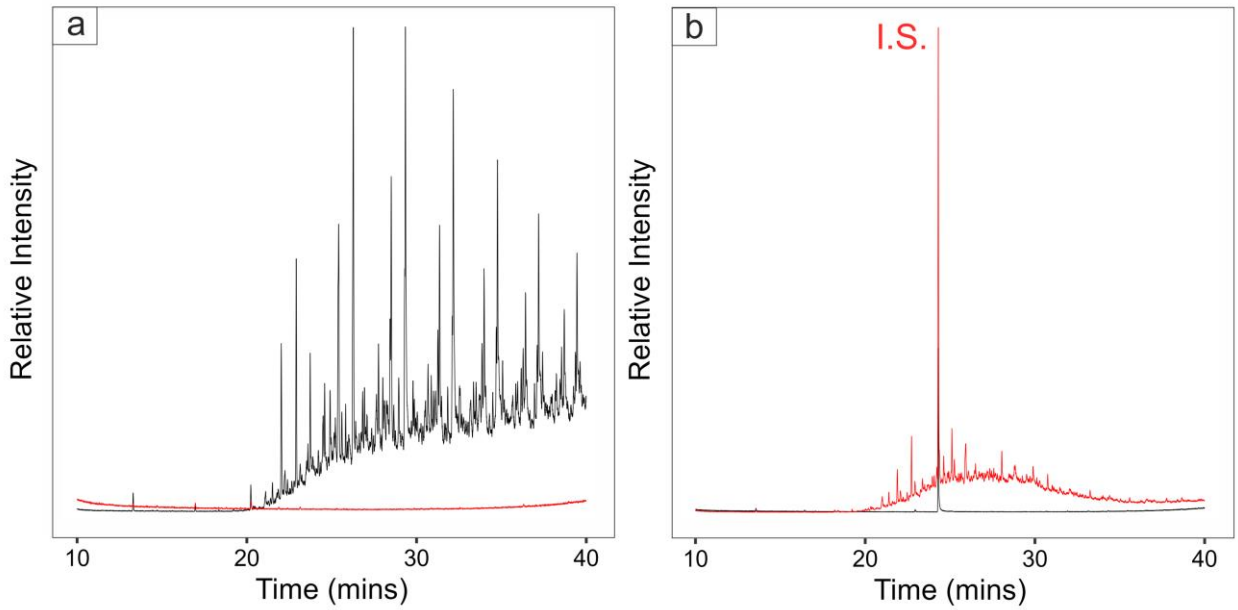

405

Fig. 5: GC-FID chromatograms **(a)** fine fraction of sand and clay blend sieved into a plastic beaker (black) and glass beaker (red) **(b)** fine fraction (<63 μm, red) and coarse fraction (>63 μm, black) of sand and clay blend sieved following disaggregation with sodium

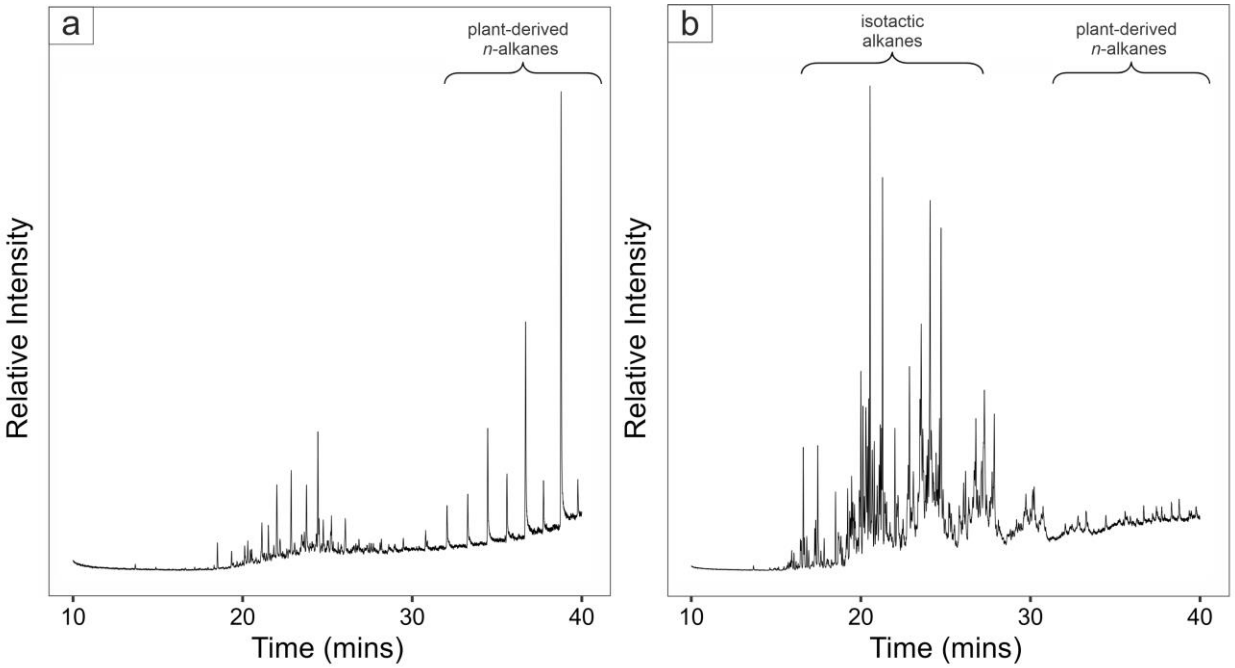

hexametaphosphate (Calgon). Large peak at 24 minutes in (b) is bromohexadecane internal standard.

Fig. 6: GC-MS chromatograms for fine fraction sediment from Hole 1168A, Core 2H (Core catcher, 17.0 MBSF). **(a)** and **(b)** apolar (*n*-alkane) fraction of sieved sediment into glass and plastic beakers respectively.

4 Discussion

4.1 Grain-size sieved sediments yield robust TEX_{86} sea surface temperatures estimates

Evidence from modern (Xiao et al., 2023) and ancient (Paleocene-Eocene Thermal Maximum; 56 million years ago) coastal marine sediments (Zachos et al., 2006) suggests that TEX_{86}-derived SST estimates are broadly similar between bulk sediment and fine grained size fractions (typically deviating between ~1 to 3°C) (Xiao et al., 2023). However, previous studies only considered two sites and thus may not be globally representative. Here, we show that the standard deviation of TEX_{86}-derived SSTs between bulk sediment and different grain-size fractions is relatively small (< 2 °C, Fig. 3.a) and that isoGDGTs are similarly distributed

between different grain-size fractions. This is observed across all sites examined here (ODP Site 1172, Site 1168, Site U1356, and Site U1451) except the coarse fraction of OPD Site 242, suggesting this is a global phenomenon in Cenozoic-aged marine sediments.

To validate this further, we compared TEX_{86} SSTs generated from bulk sediment and fine and coarse grain-size sediment fractions alongside published high-resolution TEX_{86} SST estimates generated from bulk sediment at Site 1172 (Bijl et al., 2009) and Site 1168 (Hoem et al., 2022). To ensure consistency between studies, TEX_{86} values were recalculated using the same Bayesian SST calibration and implemented identical priors (Tierney and Tingley, 2014) (Supplementary Table 2). At Site 1172, the variation between bulk and sieved sediment SST estimates (average $\Delta SST = 0.6\ °C \pm 0.5$, excluding the outlier in the late Eocene) is much smaller than the temperature variability observed in the long-term record (~10°C). At Site 1168, the variation between bulk and size sieved sediments (average $\Delta SST = 1.5\ °C \pm 1.1$) is also much less than the late Neogene cooling observed at this site. This confirms that fine and coarse grained sediment fractions can be used to infer SST evolution across major climate transitions during the Cenozoic (Fig. 7).

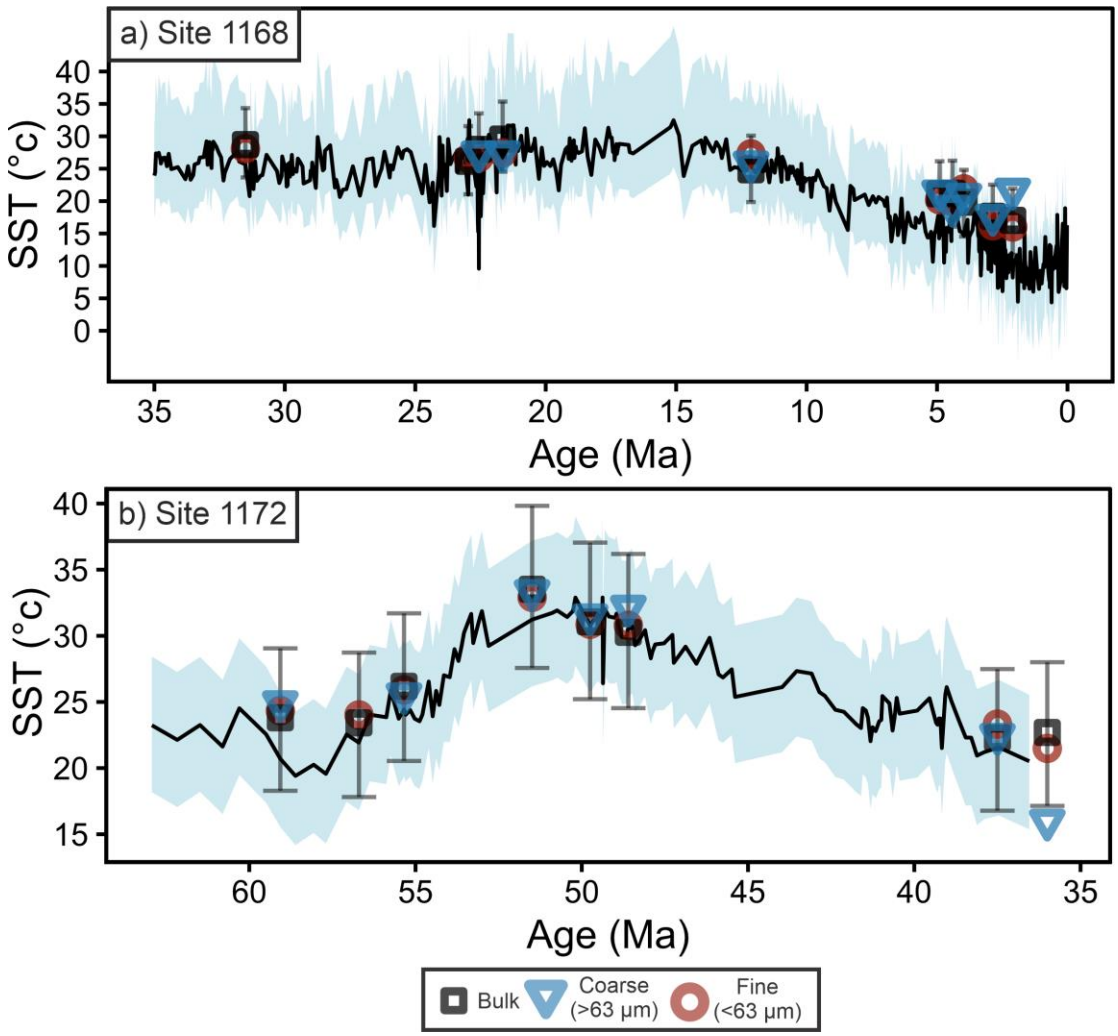

Fig. 7: Comparison of TEX_{86} SST estimates in sieved sediments (symbols) and existing high-resolution bulk sediments (black line) at (a) ODP Site 1168 (Hoem et al., 2022) and **(b)** ODP Site 1172 (Bijl et al., 2009). All SST estimates are calculated using the BAYSPAR model (Tierney and Tingley, 2014) with the 95% confidence intervals shown in blue.

4.2 Impact of grain-size sorting on the MBT'$_{5ME}$ MAT proxy

Evidence from modern coastal sediments shows that branched GDGT distributions are similar between different grain-size fractions (Yedema et al., 2024). This implies that MBT'$_{5ME}$ temperature proxy can also be applied in fine and coarse grained sediment fractions. In our global deep ocean dataset (Fig. 3), there is a linear relationship between MBT'$_{5ME}$ -derived MATs in bulk sediment and different grain-size fractions and minimal deviation in MBT'$_{5ME}$ -derived MATs between bulk sediment and grain-size sorted sediments (average deviation ±0.3

454 °C). This confirms that the brGDGT distribution is conserved between different grain-size
455 fractions and implies weak organo-mineral association (see also Yedema et al, 2024). However,
456 the relationship between bulk sediment and fine grained sediment fractions (r^2 = 0.81, p =
457 <0.001) is statistically stronger than the relationship between bulk sediment and coarse grained
458 sediment fractions (r^2 = 0.70, p = <0.001), suggesting that fine grained sediments are more
459 representative of the original bulk sediment.

460 To explore this further, we compared the grain-size sorted sediments to the published high-
461 resolution MBT'$_{5ME}$ based MAT estimates generated from bulk sediment at Site 1172 (Bijl et al.,
462 2009). At Site 1172, the variation between bulk and sieved sediment MAT estimates (average
463 ΔMAT = 0.4 °C excluding one outlier) is much smaller than the temperature variability observed
464 in a long-term higher-resolution record obtained from bulk sediment (5-7 °C) (Bijl et al., 2021).
465 Our results suggest that grain-size sorting does not overly impact brGDGT-derived MAT
466 reconstruction at Site 1172. In contrast, at Site 1168, MBT'$_{5ME}$ -derived MATs in fine or coarse
467 sediments can deviate from the bulk sediment by up to ±7 °C (Supplementary Fig. 3), suggesting
468 additional controls at this site.

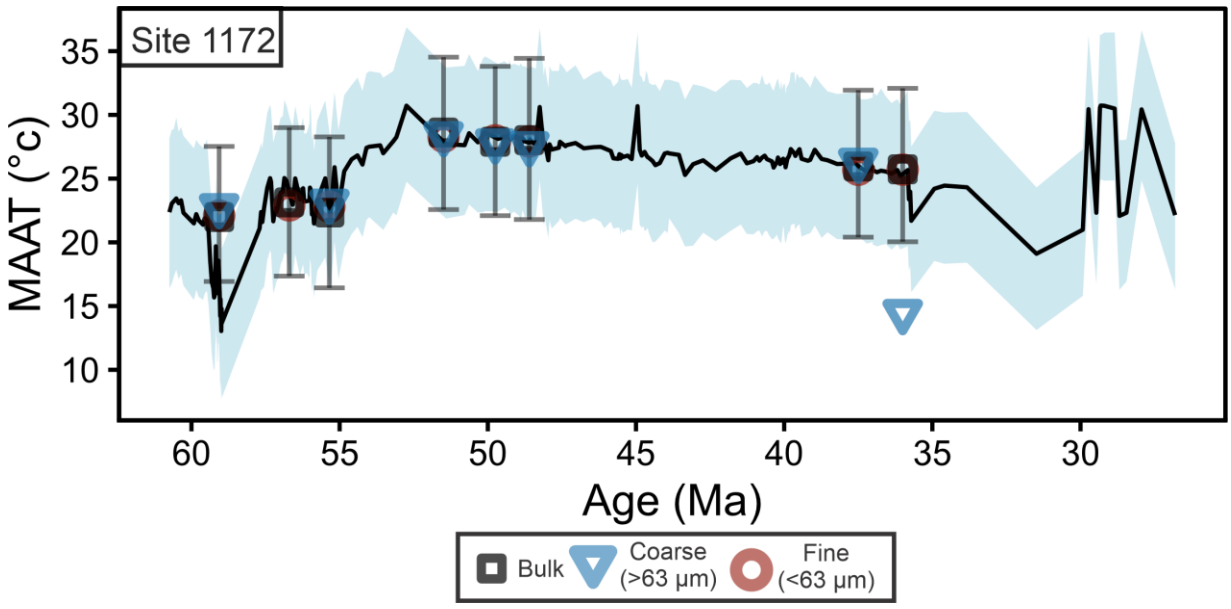

469

470

Fig. 8: MBT'$_{5ME}$ based mean annual temperature reconstruction for Site 1172. Blue band and black dashed line represent published data and associated uncertainty (Bijl et al., 2021) and circles represent the sediments studied here.

4.3 Impact of grain-size sorting on BIT indices

Terrestrial OC is often associated with fine-grain minerals (Peterse and Eglinton, 2017), such that the BIT index – representing the ratio of brGDGTs (terrestrial OC) to crenarchaeol (marine OC) – could be particularly sensitive to biases introduced during grain-size fractionation. Indeed, we show that across our analysis of the global dataset presented here, the BIT index is strongly correlated between bulk sediment and the fine-grained sediment fraction ($r^2 = 0.87$, Fig. 3) while the correlation is significantly weaker between bulk sediment and coarse-grained sediment fraction ($r^2 = 0.76$, Fig. 3). At Site 1172, the BIT index shows minimal variation across grain-sizes, indicating similar associations of crenarchaeol and brGDGTs with different grain-sizes. This explains why TEX_{86} (section 4.2) and MBT'$_{5ME}$ values (section 4.3) obtained from Site 1172 remain consistent across grain-size fractions. However, at Site 1168, deviations in the BIT index between coarse and fine grained sediment fractions are considerable compared to bulk sediments ($\Delta BIT \geq 0.5$ units). The greatest deviation occurs in samples with identified in-situ marine production (Supplementary Fig. 6) suggesting that in-situ production can lead to unreliable BIT values in grain-size-sorted sediment fractions.

4.4 Impact of grain-size sorting on *n*-alkane chain length metrics

In contemporary marine environments, CPI values in bulk sediments remain relatively consistent along a coastal transect, suggesting that *n*-alkanes do not degrade significantly during transport and deposition (Yedema et al., 2024). However, prior studies have shown that CPI values differ between grain-size fractions with higher values (relative to bulk sediment) in silt and sand fractions (30-63 µm and 63-125 µm size fractions) (Yedema et al., 2024) and similar values (relative to bulk) in clay fractions (<10 µm and 10-30 µm). Given that long-chain *n*-alkane concentrations are highest in very fine grain sediment fractions (<10 µm, 10-30 µm, Yedema et al., 2024), this suggests that *n*-alkanes are primarily bound to clay minerals. Our dataset supports

this, as there is a stronger correlation between CPI values in bulk and fine-grained sediment fractions ($r^2 = 0.59$) compared to bulk and coarse grain sediment ($r^2 = 0.09$, Fig. 4.b.). Consistent with Yedema et al. (2024), our findings indicate that CPI values for coarse grained sediment fractions generally underestimate bulk sediment CPI by up to 3-4 units (overestimating thermal maturity), suggesting that only bulk sediment or fine grain-size fractions should be used to infer CPI in ancient marine sediments.

In the experiments presented here the deviation in CPI values between bulk sediment and different grain-size fractions varies across samples, with differences reaching up to 2.4 CPI units in the fine fraction (average Δ CPI = 0.64) and up to 3.9 CPI units in coarse fractions (average Δ CPI = 1.05). However, these deviations are relatively low compared to the extensive range observed in modern plants, which can vary between 5 CPI units in graminoids to 12 CPI units in angiosperms, and even up to 30 in some cases (Bush and McInerney, 2013). In marine settings with high CPI values (e.g.,Site 1168, where CPI ranges from ~6 to 4), a difference of 1-2 CPI units would not significantly impact paleoclimate interpretations, suggesting a continuous input of thermally immature OC. However, in cases with lower CPI values (e.g.,Site U1356, where CPI ranges from ~3 to 4), a difference of 1-2 CPI units may indicate a mix of thermally immature and mature organic matter (Hollingsworth et al., 2024).

4.5 Impact of polarity on biomarker preservation in marine sediments

Our study indicates that GDGT-based climate metrics between bulk sediments and across size fractions are similar suggesting that brGDGTs and isoGDGTs do not have a strong association with mineral surfaces in aquatic environments. This finding aligns with modern studies showing that brGDGTs have a relatively weak organo-mineral association, as their distributions diminish rapidly after entering the marine water column (Yedema et al., 2024). In contrast, *n*-alkane chain length metrics differ between fine and coarse grain-sizes, exhibiting a stronger statistical relationship between *n*-alkane chain length metrics in fine sediments compared to bulk sediments, indicating a preference for *n*-alkanes to associate with mineral surfaces.

Previous hypotheses propose that more polar biomarkers (e.g.,branched and isoprenoidal GDGTs) bind weakly to mineral surfaces, while nonpolar compounds (e.g., *n*-alkanes) exhibit

stronger adhesion (Yedema et al., 2024). This is because long chain *n*-alkanes lack polar functional groups, whereas brGDGTs and isoGDGTs contain two hydroxyl groups, suggesting that lipid chemical structure strongly influences on how lipids partition into different grain-size associations. The association of different biomarkers with various clay minerals may impact their specific OC distributions. Previous research in locations such as the Gulf of Mexico (Yedema et al., 2024), the South Yellow Sea (Xiao et al., 2023), and continental margins (Lattaud et al., 2022) did not find mineralogy to be a significant factor influencing lipid biomarker grain-size distributions. Although alkenones were not detected in any of our samples, previous work has showed that $U^{K'}_{37}$ is relatively robust to sieving in modern environments (Xiao et al., 2023). It is expected that the presence of polar carbonyl groups will elicit a similar mineral association to that seen with GDGTs. However, further studies are needed to explore how various lipid biomarker compounds associate with different clay minerals in deep-time environments.

4.6 Sieving marine sediments into plastic beakers introduces extensive contamination.

In our experience, it is common that paleoclimate studies focused on inorganic geochemistry sieve marine sediments into plastic beakers. While this is not always the case, it is likely that little or no metadata will exist as to the nature of the beakers used. However, this may introduce substantive contamination into the fine fraction and may compromise organic biomarker analysis. Here, we compare the impact of sediments into glass and plastic beakers and show that multiple contaminants are introduced into the fine fraction after sieving into plastic beakers (

Fig. 5.a.). The contaminants identified here are largely a homologous series of isotactic alkanes that differ only by the presence of methyl-branches on the hydrocarbon chain. These compounds are commonly found in polypropylene (PP) beakers but crucially, resemble *n*-alkane distributions found in thermally mature sediments. The relative abundance of isotactic alkanes is sufficiently high that it can overprint the endogenous *n*-alkane signature in relatively OC-rich marine sediments (Fig. 6). The presence of a homologous series of contaminants that co-elute with plant-derived *n*-alkanes is concerning and increases the likelihood of misinterpretation when using gas chromatography alone (e.g., GC-Flame Ionisation Detection (FID)). This can be partially (but not fully) mitigated using authentic *n*-alkane standards and/or via GC-MS and mass spectral identification. Therefore, to ensure the greatest use of material recovered from the deep ocean, we recommend glass beakers are used where possible. However, if sediments are used for

subsequent boron isotopic analysis, caution must be used due to the prevalence of borosilicate glass in laboratories.

Calgon (sodium hexametaphosphate) is often used to disaggregate sediment prior to wet sieving (Feldmeijer et al., 2013) but may also introduce contamination. However, we find relatively low contamination in sediments that used Calgon but do identify an unresolved complex mixture of organic compounds in the fine fraction (

Fig. 5.b) but find no obvious contamination in the coarse fraction. The fine fraction (i.e. kaolin) is more absorbent than the coarse (i.e. sand) fraction, and therefore likely to uptake more Calgon during the mixing process. The Calgon used in this process is typically 'general purpose grade' purity, albeit with no quantification of contamination level. It is hypothesised that the same process as seen in the method blank will also occur in marine sediments as the grain-size fractions typically have a similar composition (Brooks et al., 2022).

Finally, we note that normal washing processes for sieves introduce minor contamination into the coarse grain-size fraction (Fig.5.b). To remove this contamination, sieves were sonicated using DCM:MeOH (9:1 *v*/*v*), removing cross-contamination from other samples or cleaning processes. We also tested ethanol but found this was insufficient to remove trace organic matter from the sieves. As DCM is a likely carcinogen, ethyl acetate has been proposed as a suitable, less hazardous, alternative (Diefendorf, 2025). We therefore recommend that future studies test the use of ethyl acetate to clean sieves.

Our contamination tests show that when analysing biomarkers in fine-grained sediments from legacy samples (i.e. those sieved into plastic containers), the hydrocarbon fraction can be significantly contaminated (Fig. 5.a. and Fig. 6.a.). To mitigate contamination in future work, we recommend a series of steps. Firstly, if samples have been sieved into polypropylene beakers, they should not be used for *n*-alkane analysis due to extensive leaching of isotactic alkanes and potential co-elution with endogenous plant-derived *n*-alkanes. While analysing fine fraction sediments with GC-MS can partially resolve this, it may not completely exclude overprinting. Secondly, if Calgon was used to disaggregate sediment samples, the fine fraction (<63 μm) sediment should be regarded as unsuitable for *n*-alkane analysis due to possible contamination from impure Calgon.

While homogenization can increase sediment surface area and enhance extraction efficiency in with low organic carbon content, this should also be avoided if microfossils are to be analysed post-solvent extraction, as it may damage these microfossils (Crumpton-Banks et al., 2022; Guitián and Stoll, 2021; Guitián et al., 2019). If legacy samples can be validated as minimally contaminated (i.e. by using glass beakers, avoiding Calgon and rinsing sieves with appropriate organic solvents), then *n*-alkane chain length metrics in fine (<63 μm) sediments can be deemed suitable for paleoclimate reconstruction. GDGTs appear unaffected by plastic contamination or Calgon use, yielding consistent results across most fine and coarse grain-size fractions. The lack of detectable contamination is largely attributed to the use of selected ion monitoring when analysing brGDGTs and isoGDGTs as fragmentation of contaminants is highly unlikely to produce the characteristic ions used for GDGT analysis. However, it remains crucial to avoid cross-contamination in legacy samples where sieves have not been thoroughly cleaned with appropriate solvent between samples.

In future studies where grain-size sorting is undertaken, appropriate records of the sieving container and methodology used should be recorded in the metadata. This ensures that legacy samples can be revisited and prevents plastic contamination in biomarker analysis and borosilicate contamination in $\delta^{11}B$ analysis (Green et al., 1976, Kubota et al, 2021). When boron isotopes are to be analysed, we suggest it is preferable to perform organic geochemical extraction prior to grain-size sorting because this has no apparent effect on the consequent $\delta^{11}B$ analysis (Crumpton Banks et al., 2022). However, future studies should also consider the target analytes and aim of the study. Where GDGTs are targeted, grain size sorting and the use of plastic beakers has limited impact on various GDGT metrics, indicating that sediment samples can be initially sieved for foraminifera/microfossil analysis before lipid analysis. This helps mitigate any risk of $\delta^{11}B$ contamination. However, where leaf wax metrics are targeted, grain-size sorting yields different values in different size fractions and the use of plastic beakers will introduce extensive contamination. In this instance, lipid extraction should be completed on the bulk sediment and a separate aliquot used for foraminifera/microfossil analysis.

5 Conclusions

In this study, we analysed lipid biomarker distributions in Cenozoic marine sediments to evaluate the suitability of grain-size sorted sediments for organic biomarker analysis. Our findings indicate that the isoGDGTs and brGDGTs in our experimental samples are mostly unaffected by grain-size fractionation and show relatively weak associations with organo-minerals, suggesting GDGT-based temperature proxies (e.g., TEX_{86} and MBT'_{5ME}) can effectively reconstruct past environmental conditions using either fine or coarse grain sediments, though this should ideally be assessed on a site-by-site basis. In contrast, common *n*-alkane chain length metrics used to assess changes in OC sources (e.g., CPI, ACL) in coarse-grained sediments do not accurately represent the bulk sediment and consistently underestimate CPI values by 3-4 units. Chain length metrics in fine-grained size sediments are more robust, but ideally legacy samples should be investigated on a site-by-site basis to determine the sample processing history and suitability. We also show that sediments that have previously been sieved into plastic containers should not be used for *n*-alkane analysis. Overall, our study confirms that previously sieved marine sediments – especially fine-grained sediments - can be re-evaluated for GDGT analysis, potentially providing new insights into the evolution of marine and terrestrial temperatures throughout the Cenozoic and beyond. We therefore strongly recommend that fine fraction sediment produced during grain-size sorting for micropaleontology studies should be retained and the processing method recorded to allow re-evaluation in legacy studies.

Acknowledgements

This research used samples provided by the International Ocean Discovery Program (IODP) and its predecessors. JSH acknowledges funding from the Natural Environment Research Council (NE/S007210). GNI is supported by a GCRF Royal Society Dorothy Hodgkin Fellowship (DHF\R1\191178) with additional support via the Royal Society (RF\ERE\231019, RF\ERE\210068) and NERC (NE/V018388/1). JHW receives support from the Heising-Simons Foundation. We also thank Michaela K. Reay and Megan Wilding for helpful discussions. We are grateful to Rui Bao and two anonymous reviewers for their constructive and helpful reviews of the manuscript.

Conflict of Interest Statement

The authors have no conflicts of interest to disclose

Open Research

The processed data used in this study are available at OSF and associated with a CC-By Attribution 4.0 International license (Hingley, 2025)

References

Andrady A. L. and Neal M. A. (2009) Applications and societal benefits of plastics. *Phil Trans R Soc B* **364**, 1977-1984.

Arrigoni A., Piller, W.E. and Auer, G. (2024) A new methodology for foraminifera extraction from cemented calcareous shelf sediments. *Marine Micropaleontology* **187**, 102324.

Auderset A., Moretti S., Taphorn B., Pia-Rebecca E., Kast E., Wang X. T., Schiebel R., Sigman D. M., Haug G. H. and Martinez-Garci A. (2022) Enhanced ocean oxygenation during Cenozoic warm periods. *Nature* **609**, 77-82.

Barker S., Cacho I., Benway H. and Tachikawa K. (2005) Planktonic foraminiferal Mg/Ca as a proxy for past oceanic temperatures: a methodological overview and data compilation for the Last Glacial Maximum. *Quaternary Science Reviews* **24**, 821-834.

Bijl P. K., Schouten S., Sluijs A., Reichart G.-J., Zachos J. C. and Brinkhuis H. (2009) Early Palaeogene temperature evolution of the southwest Pacific Ocean. *Nature* **461**, 776-779.

Bijl P. K., Frieling J., Cramwinckel M. J., Boschmam C., Sluijs A. and Peterse F. (2021) Maastrichtian-Rupelian paleoclimates in the southwest Pacific - a critical re-evaluation of biomarker paleotheromometry and dinoglagellate cyst paleoecology at Ocean Drilling Program Site 1172.

Boltovskoy, E. and Wright R. (1976) Recent Foraminifera. Springer, Dordrecht. https://doi. org/10.1007/978-94-017-2860-7.

Bray E. E. and Evans E. D. (1961) Distribution of *n*-paraffins as a clue to recognition of source beds. *Geochimica et Cosmochimica Acta* **22**, 2-15.

Brooks H. L., Steel E. and Moore M. (2022) Grain-Size analysis of ancient deep-marine sediments using laser diffraction *Frontiers in Earth Science* **10**, 820866.

Bush R. T. and McInerney F. A. (2013) Leaf wax *n*-alkane distributions in and across modern plants: implications for paleoecology and chemotaxonomy. *Geochimica et Cosmochimica Acta* **117**, 161-179.

Crumpton-Banks J. G. M., Tanner T., Hernández Almeida I., Rae J. W. B. and Stoll H. M. (2022) Technical note: No impact of alkenone extraction on foraminiferal stable isotope, trace element and boron isotope geochemistry. *Biogeosciences* **19**, 5633-5644.

Davtian N., Bard E., Ménot G. and Fagault Y. (2018) The importance of mass accuracy in selected ion monitoring analysis of branched and isoprenoid tetraethers. *Organic Geochemistry* **118**, 58-62.

De Jonge C., Hopmans E. C., Stadnitskaia A., Rijpstra W. I. C., Hofland R., Tegelaar E. and Sinninghe Damsté J. S. (2013) Identification of novel penta- and hexamethylated branched glycerol dialkyl glycerol tetraethers in peat using HPLC–MS2, GC–MS and GC–SMB-MS. *Organic Geochemistry* **54**, 78-82.

Dearing Crampton-Flood E., Tierney J. E., Peterse F., Kirkels F. and Sinninghe Damsté J. S. (2020) BayMBT: A Bayesian calibration model for branched glycerol dialkyl glycerol tetraethers in soils and peats. *Geochimica et Cosmochimica Acta* **268**, 142-159.

Diefendorf, A. F. (2025) Comparing lipid extraction methods on lake sediments without dichloromethane. *Organic Geochemistry* **202**, 104919.

Eglinton G. and Hamilton R. J. (1967) Leaf Epicuticular Waxes. *Science* **156**, 1322-1335.

Green H., Blincoe C. and Weeth, H.J. (1976). Boron contamination from borosilicate glass. *Journal of Agricultural and Food Chemistry* **24**, 6, 1245-1246.

Shipboard Scientific Party (2001b) Site 1168. *Proceedings of the Ocean Drilling Program, Initial Reports* **189** (eds Exon N. F., Kennett J. P., Malone M. J.).

Shipboard Scientific Party (2001b) Site 1172. *Proceedings of the Ocean Drilling Program, Initial Reports* **189** (eds Exon N. F., Kennett J. P., Malone M. J.).

Shipboard Scientific Party. (2011) Site U1356. *Proceedings of the International Ocean Discovery Program* **318**. (eds Escutia C., Brinkhuis H., Klaus A)

Feldmeijer W., Metcalfe B., Scussolini P. and Arthur K. (2013) The effect of chemical pretreatment of sediment upon foraminiferal-based proxies. *Geochemistry Geophysics Geosystems* **14**, 3996-4014.

France-Lanord C., Spiess V., Klaus A., Adhikari R. R., Adhikari S. K., Baxter A. T., Cruz J. W., Das S. K., Dekens P., Duleba W., Fox L. R., Galy A., Galy V., Ge J., Gleason J. D., Gyawali B. R., Huyghe P., Jia G., Lantzsch H., Manoj M. C., Martos Martin Y., Meynadier L., Najman Y. M. R., Nakajima A., Ponton C., Reilly B. T., Rogers K. G., Savian J. F., Schwenk T., Selkin P. A., Weber M. E., Williams T. and Yoshida K. (2016) Site U1451. *Proceedings of the International Ocean Discovery Program* **354**.

Guitián J. and Stoll H. M. (2021) Evolution of Sea Surface Temperature in the Southern Mid-latitudes From Late Oligocene Through Early Miocene. *Paleoceanography and Paleoclimatology* **36**.

Guitián J., Phelps S., Polissar P. J., Ausin B., Eglinton T. I. and Stoll H. M. (2019) Midlatitude Temperature Variations in the Oligocene to Early Miocene. *Paleoceanography and Paleoclimatology* **34**, 1328-1343.

716 Hemingway J. D., Rothman D. H., Grant K. E., Rosengard S. Z., Eglinton T. I., Derry L. A. and
717 Galy V. V. (2019) Mineral protection regulates long-term global preservation of natural
718 organic carbon *Nature* **570**, 228-231.

719 Hingley J. S. (2025) Evaluating the Reliability of Grain-size-sorted Sediments for Organic
720 Biomarker Analysis [dataset] doi.org/10.17605/OSF.IO/FXNKS

721 Hoem F., Valero L., Evangelinos D., Escutia C., Duncan B., McKay R. M., Brinkhuis H.,
722 Sangiorgi F. and Bijl P. K. (2021) Temperate Oligocene surface ocean conditions
723 offshore Cape Adare, Ross Sea, Antarctica. *Climate of the Past* **17**, 1423-1442.

724 Hoem F. S., Sauermilch I., Aleksinski A. K., Huber M., Peterse F., Sangiorgi F. and Bijl P. K.
725 (2022) Strength and variability of the Oligocene Southern Ocean surface temperature
726 gradient. *Communications Earth and Environment* **3**, 322.

727 Hollingsworth E. H., Elling F. J., Badger M. P. S., Pancost R. D., Dickson A. J., Rees-Owen R.
728 L., Papadomanolaki N. M., Pearson A., Sluijs A., Freeman K. H., Baczynski A. A.,
729 Foster G. L., Whiteside J. H. and Inglis G. N. (2024) Spatial and Temporal Patterns in
730 Petrogenic Organic Carbon Mobilization During the Paleocene-Eocene Thermal
731 Maximum. *Paleoceanography and Paleoclimatology* **39**, 2023PA004773.

732 Hopmans E. C., Schouten S. and Sinninghe Damsté J. S. (2016) The effect of improved
733 chromatography on GDGT-based palaeoproxies. *Organic Geochemistry* **93**, 1-6.

734 Hopmans E. C., Weijers J. W. H., Schefuß E., Herfort L., Sinninghe Damsté J. S. and Schouten
735 S. (2004) A novel proxy for terrestrial organic matter in sediments based on branched and
736 isoprenoid tetraether lipids. *Earth and Planetary Science Letters* **224**, 107-116.

737 Judd E. J., Tierney J. E., Lunt D. J., Montañez I. P., Huber B. T., Wing S. L. and Valdes P. J.
738 (2024) A 485-million-year history of Earth's surface temperature. *Science* **385**, eadk3705

739 Kubota, K., Ishikawa, T., Nagaishi, K., Kawai, T., Sagawa, T., Ikehara, M., Yokoyama, Y. and
740 Yamazaki, T. (2021) Comprehensive analysis of laboratory boron contamination for
741 boron isotope analysis of small carbonate samples. *Chemical Geology* **576**, 120280.

742 Kusch S., Mollenhauer G., Willmes C., Hefter J., Eglinton T. I. and Galy V. V. (2021) Controls
743 on the age of plant waxes in marine sediments - A global synthesis *Organic*
744 *Geochemistry* **157**, 104259.

745 Lattaud J., Eglinton T. I., Tallon M., Bröder L., Erdem Z. and Ausín B. (2022) Grain size
746 controls on long-chain diol distributions and proxy signals in marine sediments. *Frontiers*
747 *in Marine Science* **9**, 1004096.

748 Liu Z., Breecker D., Mayer L. M. and Zhong J. (2013) Composition of size-fractioned
749 sedimentary organic matter in coastal environments is affected by difference in physical
750 forcing strength. *Organic Geochemistry* **60**, 20-32.

751 Metcalfe B., Feldmeijer W. and Ganssen G. M. (2019) Oxygen isotope variability of planktonic
752 foraminifera provide clues to past upper ocean seasonal variability. *Paleoceanography*
753 *and Paleoclimatology* **34**, 374-393.

754 Shipboard Scientific Party (1974) Site 242 Deep Sea Drilling Project. In *Deep Sea Drilling*
755 *Project Initial Reports*.

Peterse F. and Eglinton G. (2017) Grain size associations of branched tetraether lipids in soils and riverbank sediments: Influence of hydrodynamic sorting processes. *Frontiers in Earth Science* **5**, 49.

Poynter J. and Eglinton G. (1990) Molecular Composition of Three Sediments from Hole 717c: The Bengal Fan. *Proceedings of the Ocean Drilling Program, Scientific Results* **116**, 155-161.

Schouten S., Hopmans E. C., Schefuß E. and Sinninghe Damsté J. S. (2002) Distributional variations in marine crenarchaeotal membrane lipids: a new tool for reconstructing ancient sea water temperatures? *Earth and Planetary Science Letters* **204**, 265-274.

Shipboard Scientific Party (2002) Site 1218. In *Proceedings of the Ocean Drilling Program, Initial Reports* (eds. M. Lyle, P. A. Wilson and T. R. Janecek).

Snyder and Huber (1996) Preperation techniques for use of foraminifera in the classroom. *Paleontological Society Papers*. **2**, 231-236.

Tierney J. E. and Tingley M. P. (2014) A Bayesian, spatially-varying calibration model for the TEX_{86} proxy. *Geochimica et Cosmochimica Acta* **127**, 83-106.

Weijers J. W. H., Schouten S., Spaargaren O. C. and Sinninghe Damsté J. S. (2006) Occurrence and distribution of tetraether membrane lipids in soils: Implications for the use of the TEX86 proxy and the BIT index. *Organic Geochemistry* **37**, 1680-1693.

Weijers J. W. H., Schouten S., van den Donker J. C., Hopmans E. C. and Sinninghe Damsté J. S. (2007) Environmental controls on bacterial tetraether membrane lipid distribution in soils. *Geochimica et Cosmochimica Acta* **71**, 703-713.

Xiao R., Xing L., Chen J., Wang Y., Zhong G., Zhou Y., Huo X., Ding Y. and Bao R. (2023) Spatial Discrepancy of Hydrodynamics-Driven Impacts on Organic Biomarkers Deposition and UK37' and TEX86 Temperature Proxies Applications. *Global Biogeochemical Cycles* **37**, 32022GB007648.

Xiao W., Wang Y., Zhou S., Hu L., Yang H. and Xu Y. (2016) Ubiquitous production of branched glycerol dialkyl glycerol tetraethers (brGDGTs) in global marine environments: a new source indicator for brGDGTs. *Biogeosciences* **13**, 5883-5894.

Yedema Y. W., Sangiorgi F., Trabucho-Alexandre J. P., Nierop K. G. J., Vonk J. E. and Peterse F. (2024) Influence of Organo-Mineral Associations on TerrestrialParticulate Organic Matter Dispersal in the Northern Gulf of Mexico. *Journal of Geophysical Research: Biogeosciences* **129**, e2024JG008144.

Zachos, J., Schouten, S., Bohaty, S.M., Quattlebaum, T., Slujis, A., Brinkhuis, H., Gibbs, S.J., Bralower, T.J. (2006) Extreme warming of mid-latitude coastal ocean during the Paleocene-Eocene Thermal Maximum: Inferences from TEX_{86} and isotope data. Geology, **34** (9), 737-740.

References from Supporting Information

Bijl P. K., Bendle J. A. P., Bohaty S. M., Pross J., Schouten S., Tauxe L., Stickley C. E., McKay R. M., Rohl U., Olney M., Slujis A., Escutia C., Brinkhuis H., Scientists E., Klaus A., Fehr A., Williams T., Carr S. A., Dunbar R., Gonzalez J., Hayden T., Iwai M., Jimenez-Espejo F. J., Katsuki K., Kong G. S., Nakai M., Passchier S., Pekar S. F., Riesselman C. R., Sakai T., Shrivastava P. K., Sugisaki S., Tuo S., van de Flierdt T., Welsh K. and Yamane M. (2013) Eocene cooling linked to early flow across the Tasmanian Gateway. Proceedings of the National Academy of Science 110, 9645-9650.

Bijl P. K., Frieling J., Cramwinckel M. J., Boschmam C., Sluijs A. and Peterse F. (2021) Maastrichtian-Rupelian paleoclimates in the southwest Pacific - a critical re-evaluation of biomarker paleotheromometry and dinoglagellate cyst paleoecology at Ocean Drilling Program Site 1172.

Coxall H. K., Wilson P. A., Palike H., Lear C. H. and Backman J. (2005) Rapid stepwise onset of Antarctic glaciation and deeper calcite compensation in the Pacific Ocean. *Nature* **433**, 53-57.

Dallanave E., Bachtadse V., Crouch E. M., Tauxe L., Shepherd C. L., Morgans H. E. G., Hollis C. J., Hines B. R. and Sugisaki S. (2016) Constraining early to middle Eocene climate evolution of the southwest Pacific and Southern Ocean. *Earth and Planetary Science Letters* **433**, 380-392.

France-Lanord C., Spiess V., Klaus A., Adhikari R. R., Adhikari S. K., Baxter A. T., Cruz J. W., Das S. K., Dekens P., Duleba W., Fox L. R., Galy A., Galy V., Ge J., Gleason J. D., Gyawali B. R., Huyghe P., Jia G., Lantzsch H., Manoj M. C., Martos Martin Y., Meynadier L., Najman Y. M. R., Nakajima A., Ponton C., Reilly B. T., Rogers K. G., Savian J. F., Schwenk T., Selkin P. A., Weber M. E., Williams T. and Yoshida K. (2016) Site U1451. *Proceedings of the International Ocean Discovery Program* **354**.

Fuller, M., Touchard, Y., 2004. On the magnetostratigraphy of the East Tasman Plateau Timing of the opening of the Tasmanian Gateway and paleoenvironmental changes. In: Exon, N.F., Kennet, J.P., Malone, M.J. (Eds.), The Cenozoic Southern Ocean: Tectonics, Sedimentation, and Climate Change Between Australia and Antarctica. In: Geophys. Monogr., vol. 151. AGU, Washington DC, USA, pp. 63–78.

Hartman J. D., Sangiorgi F., Salabarnada A., Peterse F., Houben A. J. P., Schouten S., Brinkhuis H., Escutia C. and Bijl P. K. (2018) Paleoceanography and ice sheet variability offshore Wilkes Land, Antarctica - Part 3: Insights from Oligocene-Miocene TEX86-based sea surface temperature reconstructions. *Climate of the Past* **14**, 1275-1297.

Ho S. L. and Laepple T. (2016) Flat meridional temperature gradient in the early Eoecene in the subsurface rather than the surface ocean. Nature Geoscience 9, 606-610.

Hoem F. S., Sauermilch I., Aleksinski A. K., Huber M., Peterse F., Sangiorgi F. and Bijl P. K. (2022) Strength and variability of the Oligocene Southern Ocean surface temperature gradient. *Communications Earth and Environment* **3**, 322.

Shipboard Scientific Party (1974) Site 242 Deep Sea Drilling Project. In *Deep Sea Drilling Project Initial Reports*.

834

835

Figure 1.

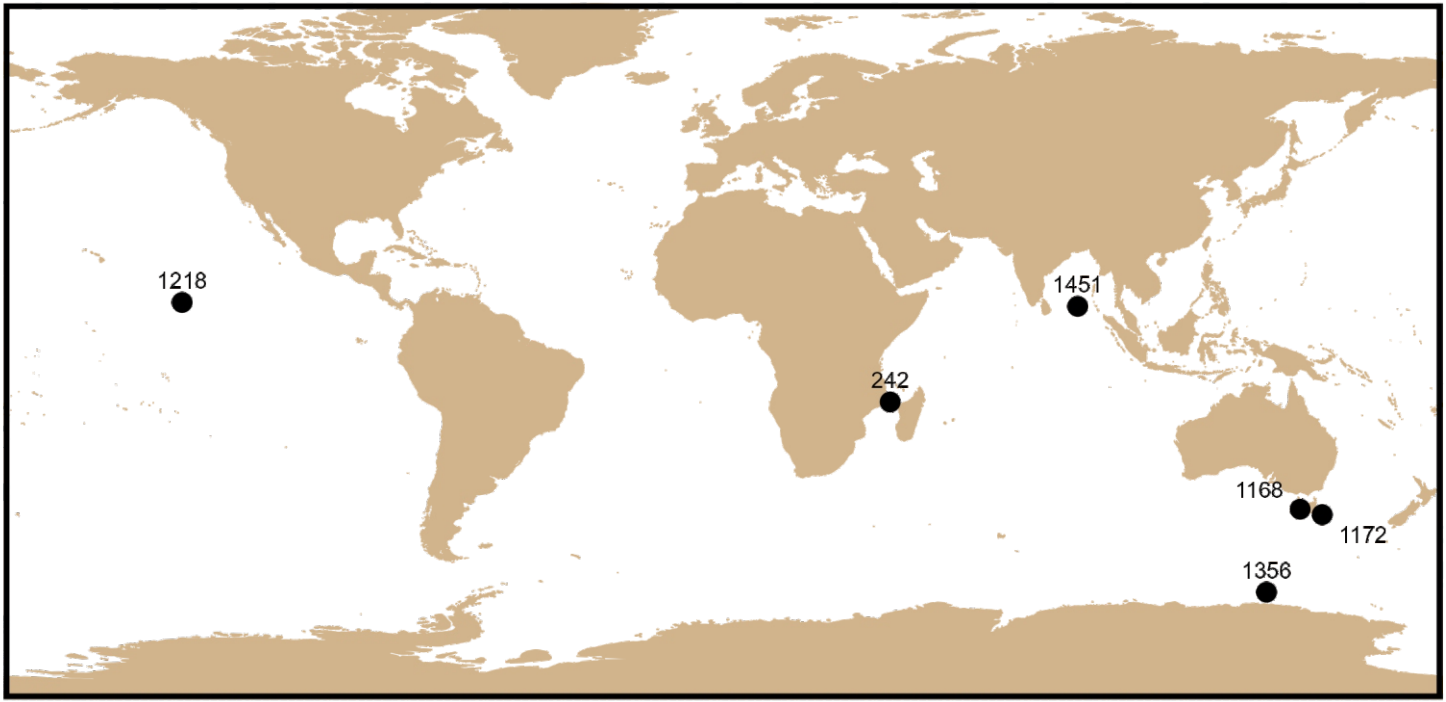
60°N
30°N
0°
30°S
60°S
1218
1451
242
1168
1172
1356
150°W
120°W
90°W
60°W
30°W
0°
30°E
60°E
90°E
120°E
150°E

Figure 2.

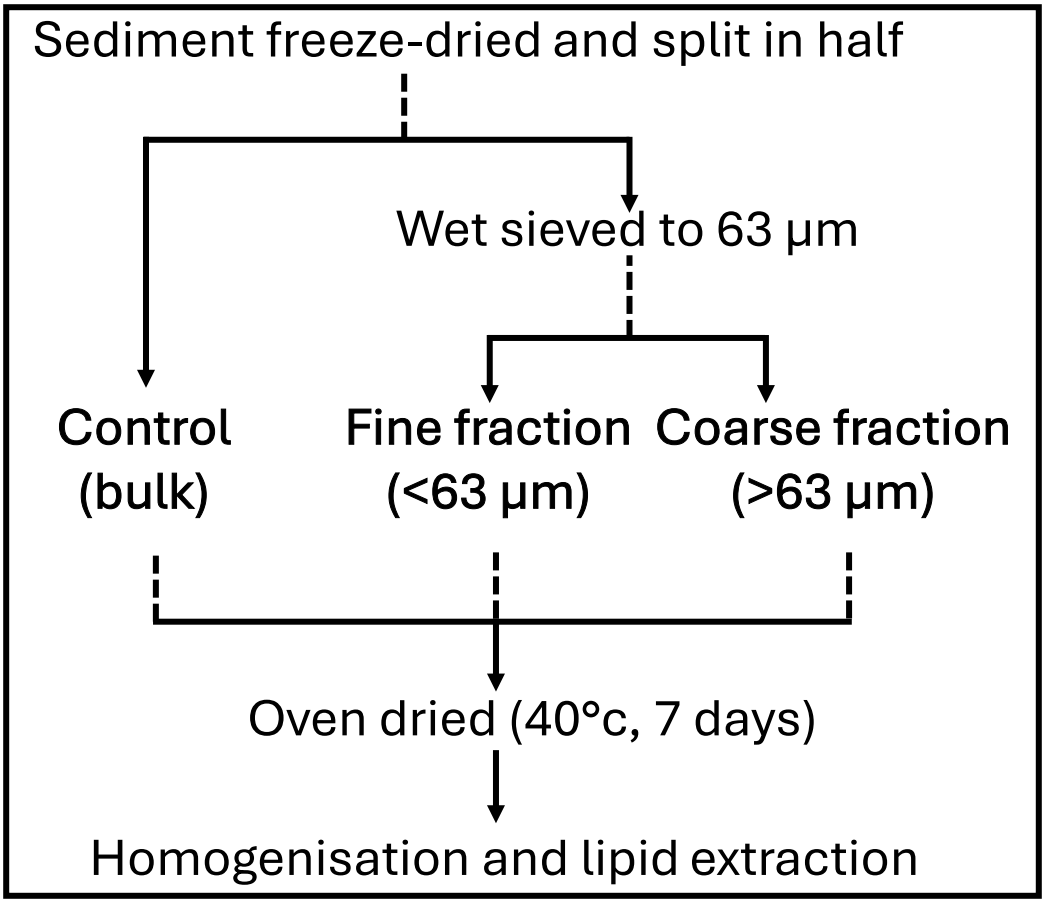
Sediment freeze-dried and split in half
Wet sieved to 63 µm
Control (bulk)
Fine fraction (<63 µm)
Coarse fraction (>63 µm)
Oven dried (40°c, 7 days)
Homogenisation and lipid extraction

Figure 3.

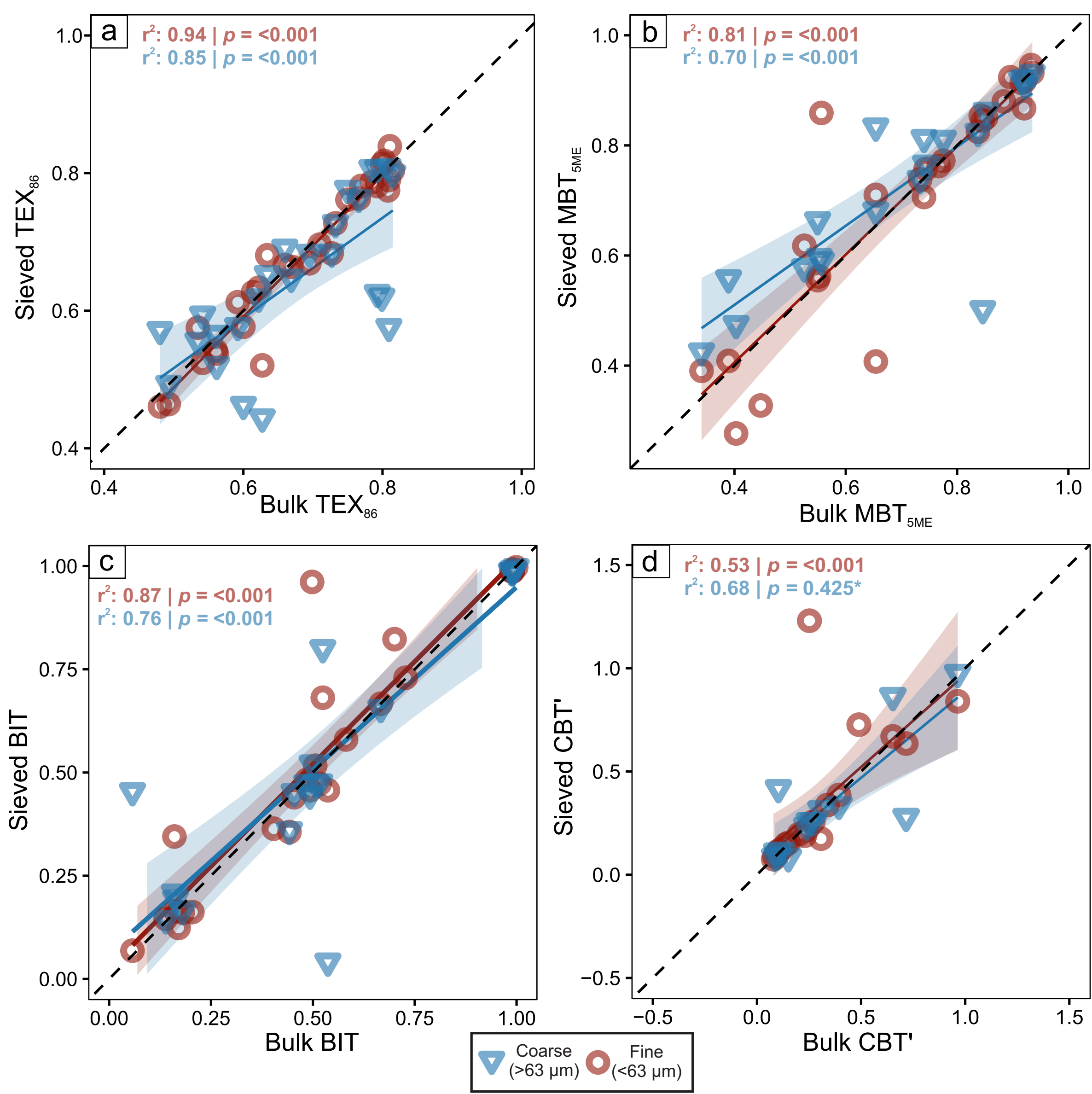
a
r²: 0.94 | p = <0.001
r²: 0.85 | p = <0.001
Sieved TEX86
Bulk TEX86
b
r²: 0.81 | p = <0.001
r²: 0.70 | p = <0.001
Sieved MBT5ME
Bulk MBT5ME
c
r²: 0.87 | p = <0.001
r²: 0.76 | p = <0.001
Sieved BIT
Bulk BIT
d
r²: 0.53 | p = <0.001
r²: 0.68 | p = 0.425*
Sieved CBT'
Bulk CBT'
Coarse (>63 µm)
Fine (<63 µm)

Figure 4.

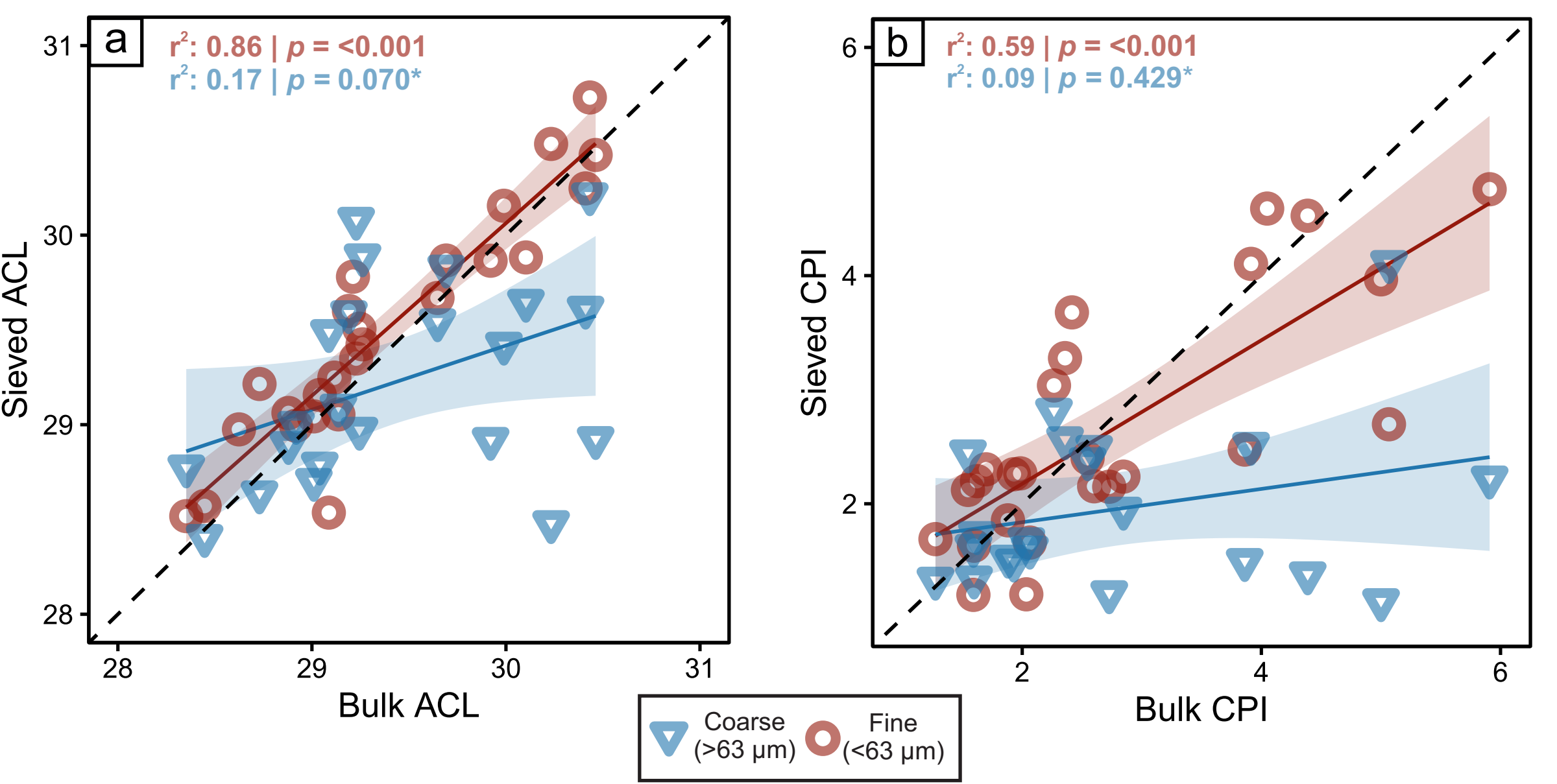
a
r²: 0.86 | p = <0.001
r²: 0.17 | p = 0.070*
Sieved ACL
Bulk ACL
31
30
29
28
28
29
30
31
b
r²: 0.59 | p = <0.001
r²: 0.09 | p = 0.429*
Sieved CPI
Bulk CPI
6
4
2
2
4
6
Coarse (>63 µm)
Fine (<63 µm)

Figure 5.

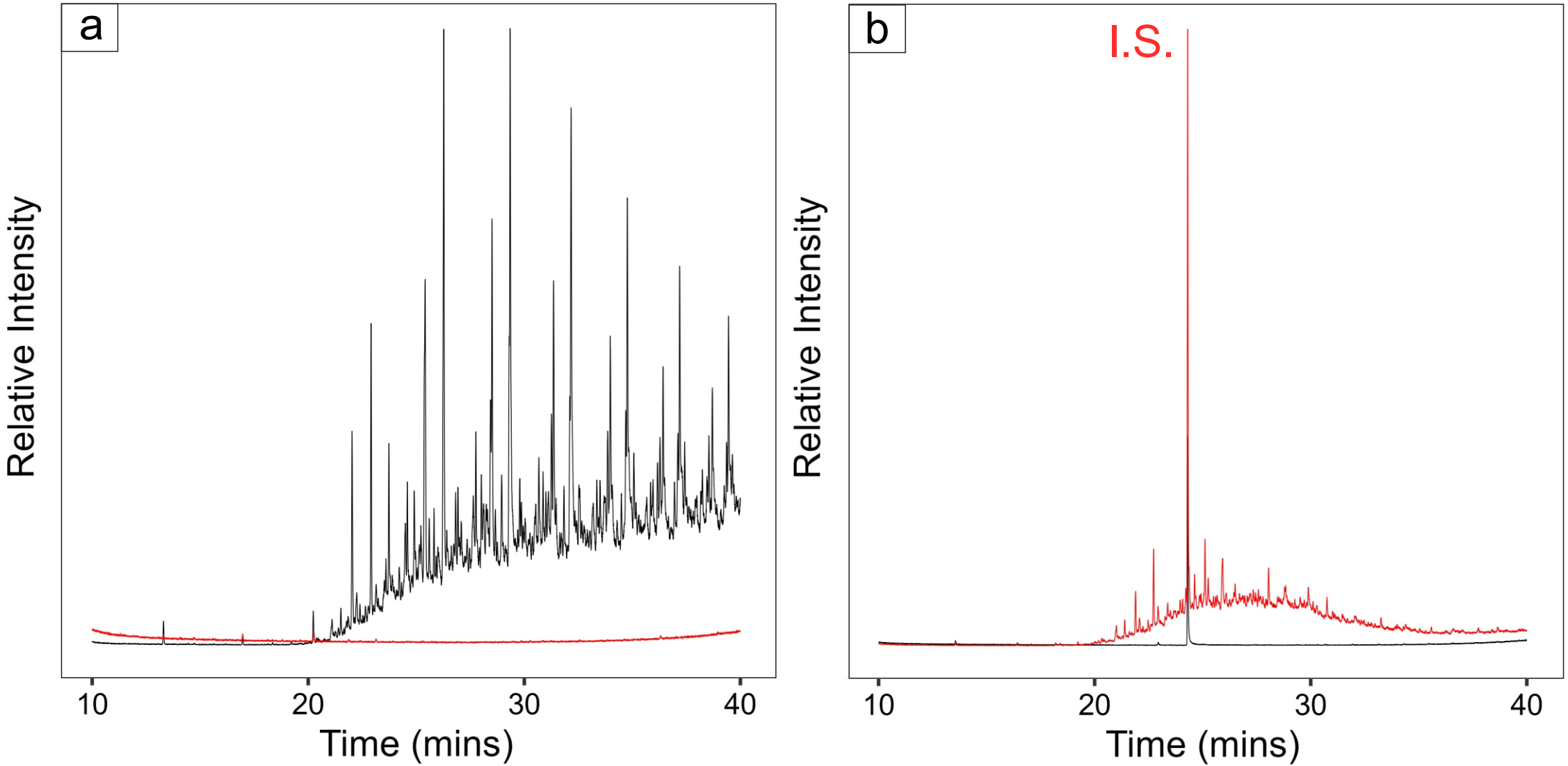
a
b
I.S.
Relative Intensity
Relative Intensity
10
20
30
40
10
20
30
40
Time (mins)
Time (mins)

Figure 6.

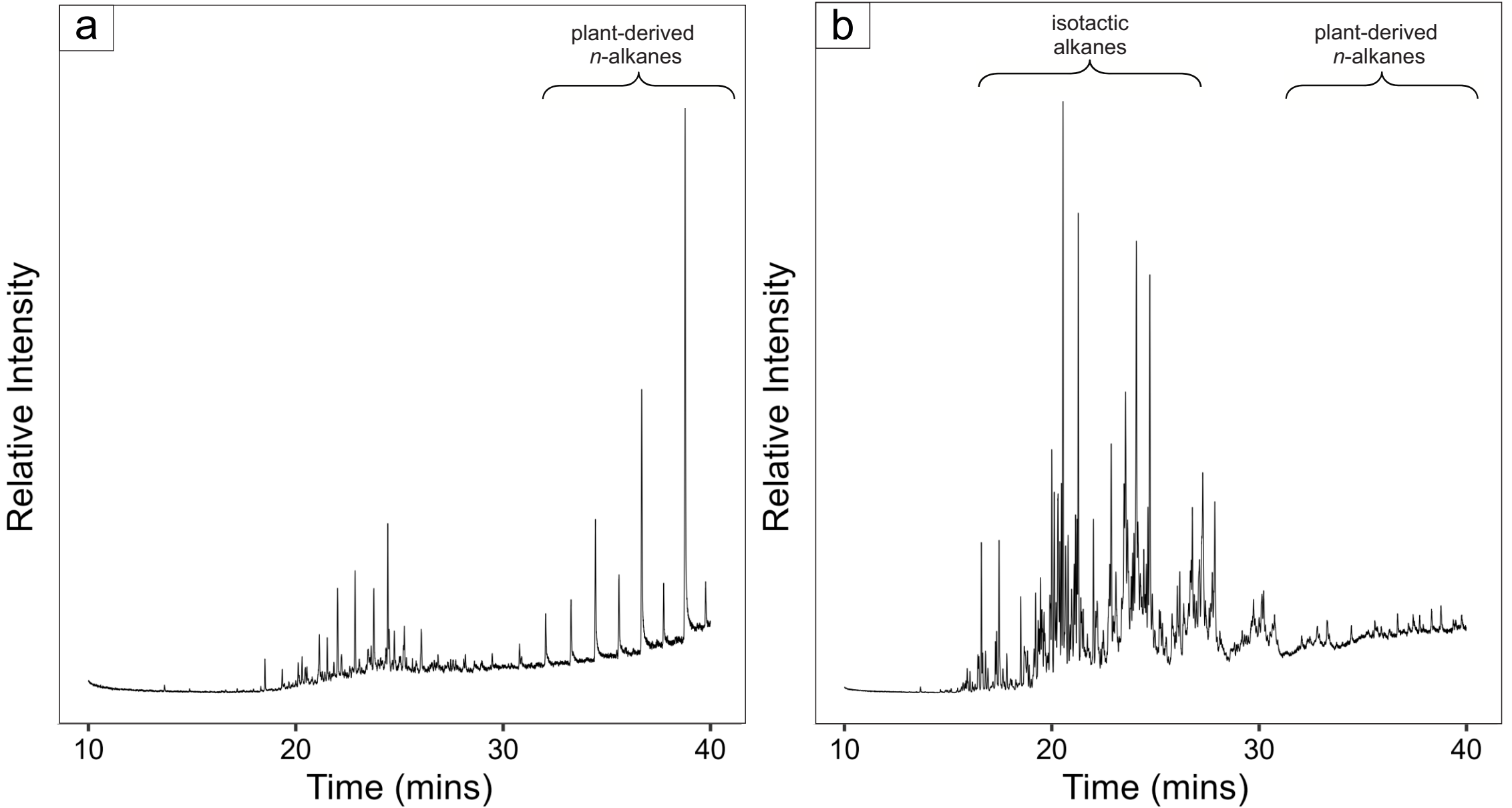
a
plant-derived
n-alkanes
Relative Intensity
10
20
30
40
Time (mins)
b
isotactic
alkanes
plant-derived
n-alkanes
Relative Intensity
10
20
30
40
Time (mins)

Figure 7.

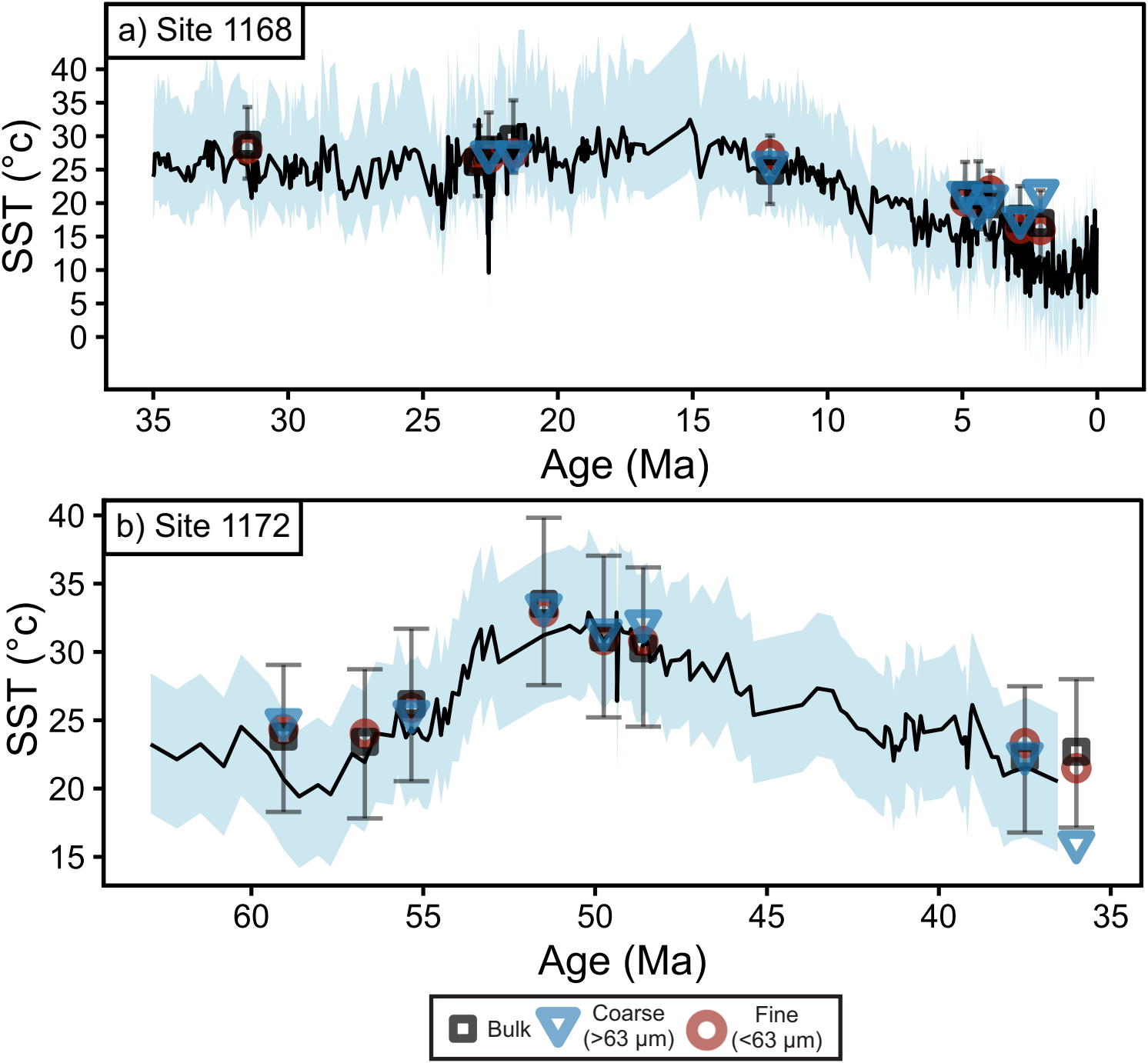
a) Site 1168
SST (°c)
40
35
30
25
20
15
10
5
0
35
30
25
20
15
10
5
0
Age (Ma)
b) Site 1172
SST (°c)
40
35
30
25
20
15
60
55
50
45
40
35
Age (Ma)
Bulk
Coarse (>63 µm)
Fine (<63 µm)

Figure 8.

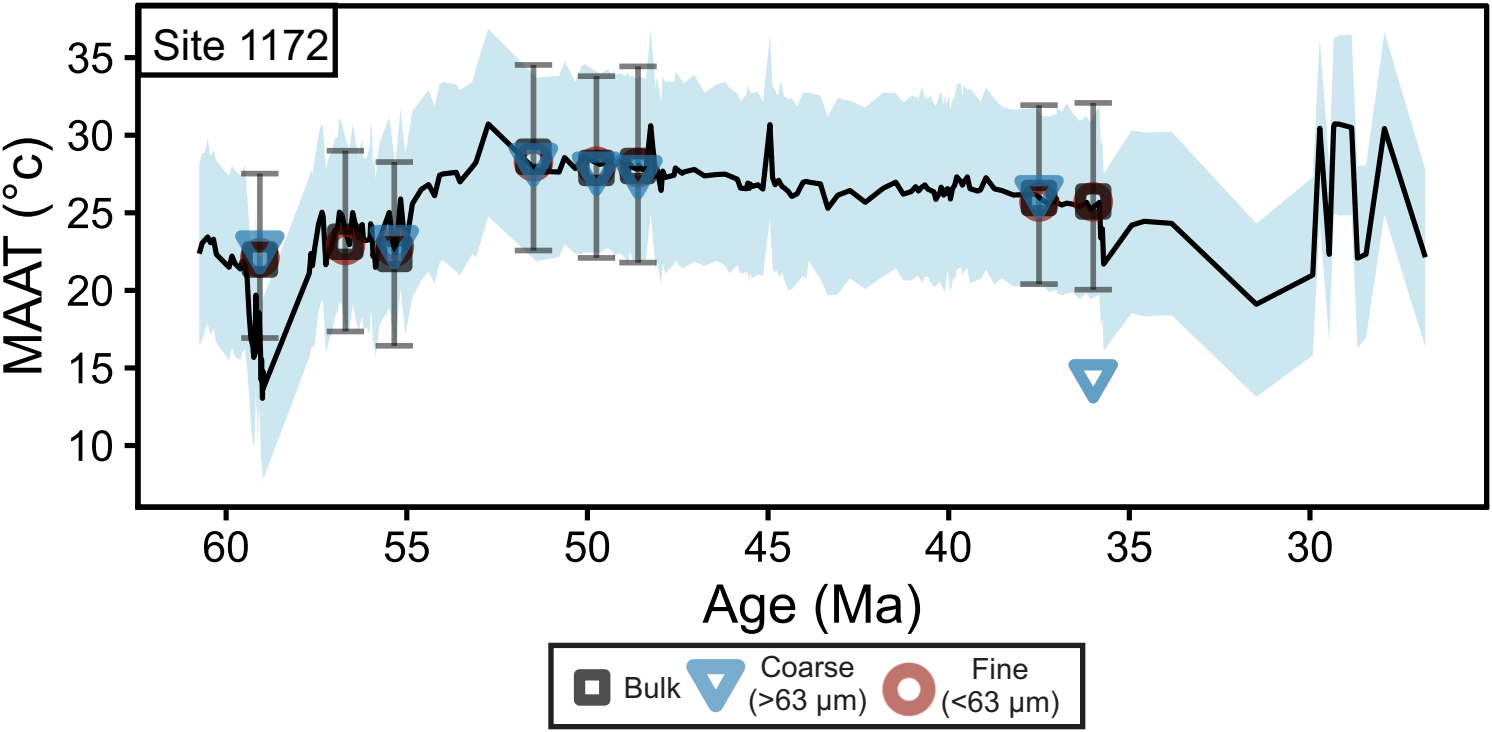
Site 1172
MAAT (°c)
35
30
25
20
15
10
60
55
50
45
40
35
30
Age (Ma)
Bulk
Coarse
(>63 µm)
Fine
(<63 µm)